Distinct Local and Global Functions of Aβ Low-Threshold Mechanoreceptors in Mechanical Pain Transmission

Mayank Gautam[1], Akihiro Yamada[2#], Ayaka I Yamada[2#], Qinxue Wu[1], Kim Kridsada[1], Jennifer Ling[2], Huasheng Yu[1], Peter Dong[1], Minghong Ma[1], Jianguo Gu[2*], Wenqin Luo[1*]

[1] Department of Neuroscience, Perelman School of Medicine, University of Pennsylvania, Philadelphia, PA 19104, USA

[2] Department of Anesthesiology and Perioperative Medicine, School of Medicine, University of Alabama at Birmingham, Birmingham, Alabama 35294, USA

[#]Equal contribution

*Correspondence: jianguogu@uabmc.edu (J.G.G.)

luow@pennmedicine.upenn.edu (W.L.)

Summary

The roles of Aβ low-threshold mechanoreceptors (LTMRs) in transmitting mechanical hyperalgesia and in alleviating chronic pain have been of great interest but remain contentious. Here we utilized intersectional genetic tools, optogenetics, and high-speed imaging to specifically examine functions of *Split*^{Cre} labeled Aβ-LTMRs in this regard. Genetic ablation of Split^{Cre}-Aβ-LTMRs increased mechanical pain but not thermosensation in both acute and chronic inflammatory pain conditions, indicating their modality-specific role in gating mechanical pain transmission. Local optogenetic activation of Split^{Cre}-Aβ-LTMRs triggered nociception after tissue inflammation, whereas their broad activation at the dorsal column still alleviated mechanical hypersensitivity of chronic inflammation. Taking all data into consideration, we propose a new model, in which Aβ-LTMRs play distinctive local and global roles in transmitting and alleviating mechanical hyperalgesia of chronic pain, respectively. Our model suggests a new strategy of global activation plus local inhibition of Aβ-LTMRs for treating mechanical hyperalgesia.

Keywords

Somatosensation; Aβ-LTMRs; intersectional genetics; optogenetics; opto-tagged electrophysiological recordings; mechanical pain; mechanical hyperalgesia, inflammatory pain; neuropathic pain; high-speed imaging; behavioral assays

Introduction

Chronic pain is a devastating disorder of the nervous system, affecting more than 30% people worldwide (Cohen et al., 2021). A prominent symptom of chronic pain is mechanical hyperalgesia (Jensen and Finnerup, 2014; Price and Gold, 2018), or increased pain triggered by mechanical stimuli. At present, effective treatment for mechanical hyperalgesia is limited, reflecting a knowledge gap in its underlying mechanisms.

Aβ-LTMRs are large-diameter, highly-myelinated, and fast-conducting primary somatosensory neurons, which normally mediate tactile, discriminative touch, and vibration sensation. Aβ-LTMRs are further divided into rapidly adapting (RA) and slowly adapting (SA) types based on their firing patterns in response to a sustained mechanical stimulus. At baseline conditions, co-activation of touch- and pain-sensing neurons inhibits the flow of nociceptive information (Arcourt et al., 2017), as proposed in the “gate control theory of pain” (Melzack and Wall, 1965).

Functions of Aβ low-threshold mechanoreceptors (LTMRs) in chronic pain have been of great interest but are controversial. On one hand, several studies suggested that Aβ-LTMRs may mediate mechanical hyperalgesia of chronic pain. Spinal nerve ligation elicited increased irregular firings of rat RA Aβ-LTMRs (Liu et al., 2000; Na et al., 1993). When activities of Aβ-LTMRs were

masked using nerve block, mechanical hyperalgesia was abolished in patients with nerve injury (Campbell et al., 1988). Spinal nerve ligation-induced mechanical allodynia in rats was abolished after destroying the dorsal column, where ascending axons of Aβ-LTMRs project through (Sun et al., 2001). Moreover, pharmacologically blocking of Aβ fiber activity relieved neuropathic pain-induced mechanical allodynia in mice (Xu et al., 2015). On the other hand, some studies suggested that Aβ-LTMRs inhibit pain transmission even in chronic conditions. Rubbing or massaging of a painful area of the skin, which presumably activates Aβ-LTMRs, attenuated pain in humans (Mancini et al., 2014). Optogenetic co-activation of nociceptors and MafA^{+} Aβ-LTMRs, as mentioned above, reduced acute pain behaviors (Arcourt et al., 2017). The spinal cord stimulator (SCS) and transcutaneous electrical nerve stimulation (TENS), which was developed based on the “gate control theory of pain” (Melzack and Wall, 1965) to target ascending axons of Aβ-LTMRs in the dorsal column (Shealy et al., 1967), are effective for treating various chronic pain conditions, including neuropathic pain (Gibson et al., 2019). Additional real-life therapy procedures, including massage therapy (Crawford and Caterina, 2020), transcutaneous electrical stimulation (Vance et al., 2012), and electroacupuncture (Duan-Mu et al., 2021), presumably involve the activation of Aβ-LTMRs for their beneficial effects.

When comparing different studies and their results, two main factors, which likely contribute to the diverse functions of Aβ-LTMRs in transmitting mechanical hyperalgesia or in its alleviation, were identified. The first consideration is the specificity of manipulating Aβ-LTMRs and the functional readouts. Though pharmacological and mechanical/electrical stimuli can inhibit or activate Aβ-LTMRs, other types of nerve fibers are likely simultaneously affected as well. For genetic and optogenetic manipulations, few available mouse genetic tools are selective or show high preference for Aβ-LTMRs (Dhandapani et al., 2018; Xu et al., 2015). Moreover, it has been challenging to differentiate touch and nociception associated reflex behavioral responses in animal studies. The second consideration is whether Aβ-LTMRs are manipulated locally at the area affected by chronic pain or in a broad manner including the unaffected Aβ-LTMRs, which may generate different sensory and behavioral outcomes.

To provide novel insight into this question, we utilized tools with improved specificity, including intersectional mouse genetics, opto-tagged electrophysiological recordings, and optogenetic activation of Aβ-LTMRs, and we performed a battery of behavioral tests to probe mouse mechanical and thermal sensations when Aβ-LTMRs were manipulated locally or globally. We also took advantage of high-speed imaging method that our lab previously established (Abdus-Saboor et al., 2019) to differentiate touch-related

non-nociceptive behavior from nocifensive behaviors. Here we found that mice with global ablation of Split^{Cre}-Aβ-LTMRs showed increased mechanical hyperalgesia in the chronic inflammatory pain condition, suggesting that Aβ-LTMRs function to inhibit mechanical hyperalgesia in chronic pain. Thermosensation was not affected by Aβ-LTMRs manipulation, indicating that these afferents functioned in a modality-specific manner. In reverse experiments, local optical activation of Split^{Cre}-Aβ-LTMRs at the hind paw triggered nociception in chronic inflammatory and neuropathic pain models. This suggests that activities of locally affected Aβ-LTMRs lead to nociception, likely contributing to mechanical hyperalgesia of chronic pain. Finally, global activation of Aβ-LTMRs at the dorsal column alleviated mechanical hyperalgesia in a chronic inflammatory pain model. Together, our results establish a new model that Aβ-LTMRs play globally inhibitory but locally promoting roles for mechanical hyperalgesia. Our model suggests a new strategy, global activation plus local inhibition of Aβ-LTMRs, for treating mechanical hyperalgesia of chronic pain.

Results

Histological and electrophysiological characterizations of *Split^{Cre}-Aβ ReaChR* mice confirmed that *Split^{Cre}* preferentially recombined in Aβ-LTMRs

To clarify functions of Aβ-LTMRs in mechanical hyperalgesia, we first established a mouse genetic strategy that would allow specific manipulation of Aβ-LTMRs. Previous studies, including our own, suggests that *Split*^{Cre} likely recombines in Aβ-LTMRs (Cui et al., 2016; Rutlin et al., 2014). We have also noticed that *Split*^{Cre} recombined in a small number of non-neuronal glia cells. Thus, we utilized an intersectional genetic strategy (Figures S1A & B) by crossing *Split*^{Cre} (Rutlin et al., 2014) and *Advil*^{FlpO} (Choi et al., 2020) mice, in which the Flippase (Flp) expression was restricted to peripheral ganglion neurons. The double heterozygous mice were then crossed with a Cre and Flp double-dependent Red-activatable Channelrhodopsin (ReaChR) reporter allele (*Rosa*$^{ReaChRf/f}$) (Hooks et al., 2015) to generate triple heterozygous *Split*^{Cre}*;Advil*^{FlpO}*;Rosa*$^{ReaChRf/+}$ (*Split*^{Cre}*-Aβ ReaChR*) mice (Figures S1A & B). Immunohistochemistry with dorsal root ganglion (DRG) sections of these mice revealed that the expression of ReaChR (tagged with YFP, recognized by anti-GFP antibodies) rarely overlapped with nociceptor markers CGRP (5.44% of GFP^{+} DRG neurons) and IB4 (4.05%) (Figure 1A) but showed high overlap with a myelinated neuron marker NF200 (89.32%) and an Aβ-LTMR marker RET (74.35%). There was also some overlap of expression with the proprioceptor marker PV (12.9%) (Figures 1B-E). Immunostaining of lumbar spinal cord sections showed that GFP^{+} central terminals did not innervate layers I/II, labeled by CGRP and IB4 staining (Figure 1F), but were enriched in deeper dorsal horn laminae (III-V), indicated by VGLUT1^{+} staining (Figure 1G)

Immunostaining of plantar skin sections showed that GFP^+ peripheral axons were $NF200^+$ (Figure 1H), and they innervate a large percentage of $S100^+$ Meissner's corpuscles (a type of RA Aβ-LTMRs, Figure 1I). Few (7.7%) GFP^+ axons innervate $K8^+$ Merkel cells (Merkel cell-neurite complex, a type of SA Aβ-LTMRs, Figure 1J & Figures S1C-F). Whole-mount immunostaining of hairy skin revealed that GFP^+ peripheral axons are $NF200^+$ (Figure S1G). A few GFP^+ fibers innervate Merkel cells in the hairy skin (Figures S1H-J), while a lot of GFP^+ fibers formed lanceolate ending structures around hair follicles (RA Aβ-LTMRs, Figures S1K-N). Together, the histological data suggest that this intersectional genetic strategy induce ReaChR expression preferentially in Aβ-LTMRs. In addition, RA Aβ-LTMRs are preferentially labeled in the glabrous skin, but RA and some SA Aβ-LTMRs are labeled in the hairy skin of these mice.

To confirm electrophysiological properties of ReaChR-labeled sensory afferents, we conducted opto-tagged electrophysiological recordings. We first performed patch-clamp recordings at the Node of Ranvier of $ReaChR/YFP^+$ fiber in isolated saphenous nerves (Figure 1K). Action potentials were evoked by electrical stimulation at the distal site of the nerves (Figure 1L), and conduction velocities were determined. The conduction velocity of $ReaChR/YFP^+$ fibers was ~20 m/s (n = 17), in the range of Aβ fibers (Figure 1M). Next, we used an ex-vivo skin-nerve preparation with both hind paw

glabrous skin and paw hairy skin and performed single-unit recordings to determine mechanical threshold and firing patterns of ReaChR/YFP^{+} fibers. ReaChR/YFP^{+} units were first identified by their responses to orange (605 nm) LED light stimuli. Mechanical stimuli by an indentator were then applied to the same receptive field as light stimuli (Figure 1N-O). A total of 7 light-sensitive saphenous nerve recordings and 9 light-sensitive tibia nerve recordings were recorded from the hairy and the glabrous skin, respectively. 4 units were RA (Figure 1P), and 3 units were SA (Figure 1Q), in the hairy skin, while 8 units were RA, and 1 unit was SA (Figure 1R) in glabrous skin. Mechanical stimulation-response curves of ReaChR^{+} units showed typical RA and SA firing patterns (Figure 1S). The mechanical thresholds of light sensitive units in the hairy and glabrous skin were similar, 1.4 ± 0.5 mN (n=11) from RA units and 3.9 ± 1.0 (n=4) from SA units (Figure 1T), which were within the threshold of LTMRs. Taken together, the electrophysiological data confirm that this intersectional genetic strategy specifically label cutaneous Aβ-LTMRs in both glabrous and hairy skin and that most of them are RA Aβ-LTMRs in the hind paw glabrous skin.

Ablation of Aβ-LTMRs by DTA treatment of *Split^{Cre}-Aβ TauDTR* mice

Next, we crossed *Split^{Cre};Advil^{FlpO}* mice to a Cre-dependent double-reporter (*Tau$^{ds\text{-}DTRf/f}$;Ai9$^{tdTomatof/f}$*) mouse line (Duan et al., 2014), containing *Tau$^{ds\text{-}DTR}$*

(the human diphtheria toxin receptor was driven by a pan neuronal *Tau* promoter) and *Ai9*^{tdTomato}. The quadruple progeny was regarded as *Split*^{Cre}-A*β TauDTR* mouse (Figure 2A). Similar to ReaChR2, the expression of tdTomato highly overlapped with large diameter neuronal marker NF200 (86.7% of tdTomato^{+} neurons), to a lesser extent with PV (12.13%), but rarely overlapped with nociceptive markers CGRP (4.02%) and IB4 (3.03%) (Figure S2A-D). Staining of lumbar spinal cord section showed that tdTomato^{+} central terminals innervate deep (VGLUT1^{+}) but not superficial (CGRP^{+} and IB4^{+}) dorsal horn laminae (Figure S2E-F). tdTomato^{+} fibers also innervated RA and SA Aβ-LTMRs in the glabrous and hairy skin (Figure S2 G-N), similar to ReaChR. Together, these histological results validated the preferential recombination in Aβ-LTMRs of *Split*^{Cre}*-Aβ TauDTR* mice.

To ablate Split^{Cre}-Aβ-LTMRs, six-week-old *Split*^{Cre}*-Aβ TauDTR* mice were intraperitoneally injected with either DTA or water (vehicle control) daily for 1 week. Two weeks after the last injection, mice were sacrificed to confirm the ablation efficiency. The numbers of tdTomato^{+} DRG neurons in whole-mount lumbar DRGs (Figures 2B & C) were quantified, and a 45.3% decrease of tdTomato^{+} DRG neurons was found after DTA treatment ($p < 0.0001$) (Figure 2D). In addition, the mean fluorescence intensity of tdTomato^{+} central terminals in the deeper dorsal horn of the lumbar spinal cord of DTA-treated mice decreased 73% ($p < 0.0001$) (Figures 2E-G). Moreover, a decrease of 81%

in tdTomato^{+} Meissiner's corpuscles-like structures in dermal papilla per foot-pad section was observed (Figures 2H-J) ($p < 0.0001$). The total number of tdTomato^{+} fibers innervating the dermal papilla also showed significant reduction following DTA treatment (vehicle = 7.57 ± 0.76 nerves/dermal papilla section, DTA = 2.38 ± 0.68 nerves/dermal papilla section, $p = 0.0022$) (Figure S2O). It is notable that the ablation phenotype of peripheral and central axons is much severer than that of the cell body, suggesting peripheral and central axon retracting in the remaining Split^{Cre}-Aβ-LTMRs. Since afferents could not function without normal peripheral or central connectivity, we considered that ~80% of Split^{Cre}-Aβ-LTMRs were functionally disrupted using this genetic and pharmacological strategy.

Ablation of Split^{Cre}-Aβ-LTMRs reduced gentle touch sensation but increased mechanical nociception in the glabrous skin

To investigate the requirement of Aβ-LTMRs in acute and chronic pain sensations, we conducted a battery of mouse behavior assays with control and ablated mice. We first examined general locomotor behavior of mice with the open field test (Figure S3A). Ablation of Split^{Cre}-Aβ-LTMRs did not significantly alter the time spent in peripheral (vehicle = 1098 ± 16.7 s vs DTA = 1075 ± 15.7 s, $p = 0.38$) and central zones (vehicle = 103 ± 16.8 s vs DTA = 125.3 ± 15.8 s, $p = 0.328$). There was also no significant difference between the two

groups in the total distance travelled (vehicle = 62.32 ± 3.1 m vs DTA = 64.05 ± 4.0 m, $p = 0.72$). These results suggest that ablation of Split^{Cre}-Aβ-LTMRs do not significantly change mouse general locomotor functions or generate obvious anxiety-associated behaviors. Next, we tested mechanosensitivity of mouse hind paws of control and ablated mice (Fig. 3A). Ablation of Split^{Cre}-Aβ-LTMRs did not alter 50% paw-withdrawal mechanical threshold (PWT, static mechanosensitivity, vehicle = 0.99 ± 0.005 g, DTA = 0.98 ± 0.007 g, $p > 0.99$, n = 9 mice) (Figure 3B) measured by the von Frey hair (VFH) test. A likely reason for no change of 50% PWT in the ablated mice is that other types of mechanosensory afferents in the hind paw, such as SA Aβ-LTMRs and MrgprD+ afferents, are largely spared by this genetic strategy. On the other hand, sensitivity to dynamic gentle touch, measured as the percentage paw withdrawal in response to by a dynamic cotton swab (Figure 3C), was significantly attenuated in the ablated mice (vehicle = 91.11 ± 4.84% vs DTA = 51.11 ± 8.88%, $p = 0.0014$, n = 9 mice). The ablated mice also spent a significantly longer time attempting to remove a sticky tape attached to the paw, which generated small amounts of mechanical forces (vehicle = 87.6 ± 14.33 s vs DTA = 198.1 ± 32.74 s, $p = 0.0063$, n = 10 mice) (Figure 3D and supplementary video 1). Together, these results suggest that the ablated mice are less sensitive to dynamic gentle mechanical forces. Moreover, when mice were tested using a chamber with different floor textures, hook (rough) vs loop (smooth) (Figure S3E), the texture preference was altered in the ablated mice.

Compared to control mice, which showed no significant preference for the floor textures (Hook = 386.5 ± 23.38 vs Loop = 478.4 ± 56.54 seconds, $p = 0.505$), the ablated mice preferred to stay in the smoother loop surface compartment (Hook = 323.9 ± 36.95 vs Loop = 559.9 ± 26.59 seconds, $p = 0.001$, $n = 8$ (vehicle) and 7 (DTA) mice) (Figure 3E). In short, the behavioral deficits in dynamic gentle mechanical forces and tactile discrimination of DTA-treated mice supported significant functional disruption of Aβ-LTMRs in these mice.

Next, we tested mechanical nociception at the paw. In response to an alligator clip at the plantar skin, licking episodes, which reflect mouse nociception, significantly increased in the ablated mice (vehicle = 4.6 ± 1.01 episodes/1 min. vs DTA = 13.8 ± 1.98 episodes/1 min., $p = 0.0002$, $n = 10$ mice in each group, Figure 3F and supplementary video 2). This result suggests that Aβ-LTMRs function to inhibit mechanical pain sensation and that disruption of Aβ-LTMR functions results in mechanical hyperalgesia. In contrast, no difference in thermal nociception, tested by static hot plate (Figure S3B), dynamic hot plate (Figure S3C), and dry ice test (Figure S3D) (see also supplementary table S1), was found between the two groups, suggesting that Aβ-LTMRs inhibits nociception in a modality-specific manner.

Moreover, we tested mechanical and heat hyperalgesia in a CFA-induced inflammatory pain model. In contrast to the baseline condition, the ablated mice showed significant reductions in 50% PWT (Figure 3G), indicating an increased mechanical nociception. The PWT significantly decreased in DTA-treated mice at 2h (vehicle = 0.54 ± 0.12 g vs DTA = 0.05 ± 0.14 g, $p = 0.0149$), 14th day (vehicle = 0.18 ± 0.06 g vs DTA = 0.037 ± 0.007 g, $p = 0.0427$), 21st day (vehicle = 0.38 ± 0.12 g vs DTA = 0.049 ± 0.015 g, $p = 0.0012$), and 28th day (vehicle = 0.694 ± 0.086 g vs DTA = 0.052 ± 0.018 g, $p = 0.0012$). The differences at days 1, 3, and 7 were not significant due to the floor effect (the PWTs of control mice were already close to 0). Interestingly, the ablated mice showed no significant change in thermal hyperalgesia (Figure 3H), which further supported the modality-specific function of Aβ-LTMRs. Together, these behavior results suggest that in the glabrous skin, disruption of $Split^{Cre}$-Aβ-LTMRs reduces the dynamic gentle-touch sensitivity and specifically dis-inhibits mechanical pain transmission at baseline and chronic inflammatory conditions.

Ablation of $Split^{Cre}$-Aβ-LTMRs altered gentle touch sensation and mechanical nociception in the hairy skin

The hairy skin contains Aβ-LTMRs as well as C- and Aδ- LTMRs (Figure S4A) (Li et al., 2011). Thus, behavior outcomes from the hairy skin of ablated mice

could be more complicated than the glabrous skin. We conducted a similar sticky tape test, which generated gentle mechanical stimuli at the de-haired back skin. The ablated mice displayed significantly increased scratching behavior in response to the tape (vehicle = 0.181 ± 0.181 scratch bouts / 5 min vs DTA = 11 ± 3.964 scratch bouts / 5 min, $p = 0.0027$, n = 11 and 10 mice in vehicle and DTA groups, respectively) (Figure S4B), but no difference in back-attending episodes between the vehicle and ablated groups (vehicle = 17.64 ± 3.8 attending episodes / 5 min vs DTA = 19.2 ± 3.552 attending episodes / 5 min, $p = 0.743$) was observed (Figure S4C). These results suggest that the ablated mice show increased responses to gentle mechanical forces at the hairy skin, which might be mediated by dis-inhibited C- and/or Aδ-LTMRs. In addition, in response to the application of an alligator clip at the nape of the neck, the ablated mice displayed significantly increased number of attending episodes (vehicle = 8.45 ± 1.60 vs DTA = 17.4 ± 2.16 attending episodes / 1 min, $p = 0.0074$, n = 11 and 10 mice in vehicle and DTA groups, respectively) (Figure S4D and supplementary video 3), indicating an increased mechanical pain sensation. No difference in heat nociception between the groups was found, tested by tail-immersion assay at different temperatures (supplementary table S1). These data indicate that Split^{Cre}-Aβ-LTMRs are required to “gate” both gentle touch and mechanical pain transmission in the hairy skin.

Local optogenetic activation of Split^{Cre}-Aβ-LTMRs evoked nocifensive behaviors in chronic inflammatory and neuropathic pain models

Our results using the ablated mice revealed functions of Aβ-LTMRs in specifically inhibiting mechanical pain transmission. Since multiple studies also suggested functions of Aβ-LTMRs in transmitting mechanical hyperalgesia (Campbell et al., 1988; Ishibashi et al., 2022; Tashima et al., 2018; Xu et al., 2015), we conducted reverse experiments using optogenetic activation of Aβ-LTMRs. Peripheral optogenetic stimulation of *Split^{Cre}-Aβ ReaChR* mice (Figure 4A) would activate a small population of Aβ-LTMRs innervating the skin area covered by the blue laser light. We first tested different intensities (5, 10, and 20 mW) of blue laser (473 nm) over several skin areas, the paw, nape of the neck, back and tail, to characterize spontaneous laser-evoked behaviors using a high-speed camera (Abdus-Saboor et al., 2019; Abdus-Saboor and Luo, 2022) (Figure S5A). *Split^{Cre}-Aβ ReaChR* mice were very responsive to peripheral laser stimuli. They showed ~40-90% hind paw withdrawal responses (Figure 4B), and ≥80% responses at hairy skin with different intensities (Figure S5B). The paw withdrawal latency (PWL) and the tail flick latency decreased in an intensity-dependent manner (Figures 4D, S5C and supplementary table S2).

To differentiate nocifensive or non-nocifensive paw withdrawal reflexes, we used a “pain score” system (paw guarding, paw shaking, jumping, and eye grimace) that we previously established with high-speed imaging (Abdus-Saboor et al., 2019). Laser at all intensities triggered paw withdrawal reflex (Figure 4B), but paw withdraw reflexes evoked by 5 mW blue laser did not show nocifensive features (pain score: 0 ± 0 (5 mW), 0.2 ± 0.08 (10 mW), and 0.74 ± 0.13 (20 mW)) (Figure 4C and supplementary video 4). Interestingly, after CFA-induced inflammation, 5 mW blue laser triggered a significantly higher percentage of paw withdrawal response and a significant reduction of PWLs (Figures 4E and 4G), indicating that the same stimuli evoked stronger responses of Split^{Cre}-Aβ-LTMRs in chronic inflammatory pain condition. In addition, 5 mW blue laser triggered responses with significantly higher pain scores at 2h ($p = 0.037$), days 1 ($p = 0.0022$), 3 ($p = 0.05$), 7 ($p < 0.0001$), 14 ($p = 0.0005$), 21 ($p = 0.018$), and 28 ($p = 0.017$) post CFA injection (Figure 4F, supplementary video 5 and supplementary table S2), suggesting that activation of Aβ-LTMRs triggers nociception in chronic inflammatory pain condition.

In addition, we performed conditioned place preference (CPP) assay (Fig. 4H), using littermate control mice treated with CFA, *Split^{Cre}-Aβ ReaChR* mice treated with saline, and *Split^{Cre}-Aβ ReaChR* mice treated with CFA and paired

one side of chamber with plantar optogenetic stimulation (5mW, 10Hz). *Split^{Cre}-Aβ ReaChR* mice with CFA but not the two control groups showed a significant increase of aversion (Saline = -0.77 ± 8.69 vs CFA = -41.88 ± 8.3, $p = 0.004$) towards the blue laser-paired chamber (Figures 4 I). This finding indicates that local optogenetic stimulation of Split^{Cre}+ Aβ-LTMRs in inflammatory pain condition triggered aversion.

Activation of Aβ-LTMRs was also tested in chronic neuropathic pain using the medial plantar nerve ligation (MPNL) model (Figure S5L)(Sant'Anna et al., 2016). Similarly, 5 mW blue laser triggered a significantly higher percentage of paw withdrawal response, significantly reduced PWLs (Figures 4J, 4L supplementary table S2), and significantly higher pain scores at days 1 ($p = 0.0292$), 3 ($p < 0.0001$), 7 ($p < 0.0001$), 14 ($p < 0.0001$), 21 ($p < 0.0001$) and 28 ($p < 0.0001$) post-surgery (Figure 4K and supplementary table S2). Together, our results suggest that local activation of Aβ-LTMRs triggers nociception in both chronic inflammatory and neuropathic pain conditions.

Changes in electrophysiological properties of Split^{Cre}-ReaChR^{+} Aβ-LTMRs following CFA-induced inflammation

To determine changes in firing properties of Split^{Cre}-ReaChR^{+} Aβ-LTMRs in chronic pain condition, we performed opto-tagged recording of these afferents in saline- or CFA-treated mice at post-injection Day 7. Mechanically-evoked RA impulses were recorded from light-sensitive (ReaChR/YFP tagged) afferent fibers that innervate the glabrous skin of hind paws (Figure 5A). We detected RA impulses of light-sensitive afferent fibers in both saline- (n = 7) and CFA-injected (n = 5) mice. The number of impulses increased proportionally with higher mechanical force in CFA-treated groups, which was significant at 30 ($p < 0.05$) and 80 ($p < 0.001$) mN force (Figure 5B). Similarly, we detected tissue indentation induced SA impulses in light-sensitive afferent fibers of saline- (n = 1) and CFA-injected (n = 6) mice. Though the number of Split^{Cre}-ReaChR^{+} Aβ afferents displaying SA property in control mice (n = 1) is too low for a meaningful statistical comparison, an obviously higher number of Split^{Cre}-ReaChR^{+} Aβ afferents displaying SA property after CFA treatment (n = 6) was observed (Figure 5C).

The percentages of opto-tagged afferents showing RA and SA responses were quantified. In the glabrous skin of the control mice, few light-sensitive afferents were SAs (n = 1), and most of them were RAs (n = 7), similar to the result of naïve animals (Figure 1R). However, with CFA-induced inflammation, the percentage of RA afferents (n = 5) decreased while that of SA (n = 6) increased significantly ($p = 0.05$) (Figure 5E). Mechanical thresholds of RA

afferents in control and CFA groups did not alter significantly (Figure 5F). Mechanical thresholds of SA afferents in both groups were also similar (Figure 5G). Overall, these data suggest that in chronic inflammation, the electrophysiological properties of many RA Aβ-LTMRs became SA-like, which could be one of the underlying mechanisms for triggering stronger local activity and inducing mechanical hyperalgesia in the CFA model.

To determine whether ReaChR^{+} LTMRs increased firing was due to an alteration in peripheral end organ innervation, we performed foot pad section immunostaining for ReaChR^{+} afferents, Merkel cells (Figures S5D-E), and Meissner's corpuscles (Figure S5F-G) using control or CFA-treated *Split^{Cre}*-A*β ReaChR* mice at post-CFA Day 7. We found that the number of Merkel cells per foot pad skin section showed no significant difference between groups (control = 13.02 ± 2.58 vs CFA = 9.45 ± 1.53, p = 0.18) (Figure S5H), nor did the percentage of GFP^{+} fibers innervating Merkel cells per foot pad section (control = 10.38 ± 2.37% vs CFA = 17.21 ± 2.95%, p = 0.088) (Figure S5I). The number of Meissner's corpuscles per foot pad section showed a non-significant decrease trend in CFA-treated mice (control = 4.496 ± 0.51 vs CFA = 2.89 ± 0.60, p = 0.093) (Figure S5J). Interestingly, the percentage of GFP^{+} fibers innervating Meissner's corpuscles per foot pad section significantly decreased in CFA-treated mice (control = 69.42 ± 7.87% vs CFA = 46.17 ± 5.37%, p = 0.041) (Figure S5K). Thus, our results suggest that some

Split^{Cre}-ReaChR^{+} afferents retract from Meissner's corpuscles in the inflammatory paw. This structural alternation, loss of corpuscles (Gray and Matthews, 1951), might contribute to the increased firings of Split^{Cre}-ReaChR^{+} RA afferents in the CFA model.

Dorsal column stimuli of Split^{Cre}-ReaChR^{+} Aβ-LTMRs activated spinal cord dorsal horn inhibitory neurons

How could both global ablation and local activation of Aβ-LTMRs promote mechanical hyperalgesia? We speculated that the mechanism came from the unique morphologies and circuits associated with Aβ-LTMRs**.** In contrast to nociceptors, which have central terminals innervating only one to two spinal cord segment (Olson et al., 2017; Scott, 1992), Aβ-LTMRs have ascending and descending axons projecting through the dorsal column and 3rd order collaterals covering the dorsal horn of 6 to 8 spinal cord segments (3 to 4 segments along both ascending and descending axons) (Brown et al., 1991; Niu et al., 2013). This anatomical feature allows an Aβ-LTMR to "gate" nociceptors (inter-modal crosstalk) or other Aβ-LTMRs residing in 3 to 4 dermatomes away (inter-somatotopic crosstalk) (Figure 7). Thus, even though locally affected Aβ-LTMRs are sensitized to trigger nociception in inflammation or nerve injury regions, the overall effect of all Aβ-LTMRs, most of which are unaffected, is still to inhibit mechanical pain transmission.

If our model is correct, then the global activation of Aβ-LTMRs, even in chronic pain, theoretically should still inhibit mechanical hyperalgesia. To test this idea, we implanted light-cannula above the T11 dorsal column of the spinal cord of *Split^{Cre}-Aβ ReaChR* mice (Figure 6A). Similar to the peripheral experiments, we first tested blue laser light at four different intensities, 0.5 mW, 3 mW, 5 mW, and 10 mW, at the baseline condition. During light stimuli (15 minutes total, 30 second on (10 Hz) and 1 minute off, 10 cycles), all intensities triggered some spontaneous behaviors (supplementary table S3). These behaviors calmed down to the resting state when light was off. We then did VFH test to measure 50% PWT at different time points afterwards (Fig. 6A), using blue laser at the low (0.5 mW) or high (10 mW) intensities (Fig. 6B). We averaged PWT of both paws for quantification as the light cannula was implanted at the dorsal column and would affect both sides of the spinal cord. 0.5 mW blue laser spinal cord stimuli did not significantly alter the hind PWT (supplementary table S3, Figure 6B). Thus, it was chosen to test functions of dorsal column activation of Aβ-LTMRs.

The T11 dorsal column stimuli should activate a large population of Aβ-LTMRs, whose ascending and descending axons primarily projected through the dorsal column, and their downstream neurons in the spinal cord dorsal horn (DH). If so,

DH interneurons at the lumbar enlargement, where hind paw mechanical hyperalgesia are transmitted, would also be affected. To test this idea, we performed c-Fos immunohistochemistry using T11 and L4 spinal cord sections 90 minutes after dorsal column stimuli (Figure S6 A-P). We found that the number of c-Fos^{+} cells significantly increased at both T11 and L4 spinal cord DH with light stimulation of *Split^{Cre}-Aβ ReaChR* mice, in comparison to no light stimuli control mice. Quantification of c-Fos^{+} neurons in the superficial and deep dorsal horn laminae revealed that a significant increase in the number of c-Fos^{+} neurons was found in deeper layers (T11: 4.1 ± 0.4 (No light), 16.1 ± 1.0 (Light), $p < 0.0001$; Lumbar: 3.5 ± 0.3 (No light), 16.3 ± 1.3 (Light), $p < 0.0001$) but not in superficial layers (T11: 6.2 ± 0.6 (No light), 9.1 ± 1.3 (Light), ns; Lumbar: 7.4 ± 0.4 (No light), 9.8 ± 1.5 (Light), ns) (Figure 6C).

To further discern whether the activated DH neurons are excitatory or inhibitors, we performed RNAScope *in situ* hybridization of *cFos*, *Vglut2* and *Vgat* (Figures 6D and S6M-P). Around 80% cFos+ neurons were VGAT+ (Figure 6E). Together, our results suggested that dorsal column stimuli of Split^{Cre}-ReaChR^{+} Aβ-LTMRs would preferentially activate DH inhibitory interneurons in a broad range of spinal cord levels.

Dorsal column activation of Split^{Cre}-ReaChR^{+} Aβ-LTMRs alleviated mechanical hyperalgesia of chronic inflammatory pain

Lastly, we tested whether dorsal column stimuli of Split^{Cre}-ReaChR^{+} Aβ-LTMRs using 0.5 mW blue laser attenuated or enhanced nociception in CFA-induced chronic inflammatory pain model. One hindpaw of dorsal column implanted *Split^{Cre}-ReaChR* mice were injected with CFA. The same light stimuli and VFH tests (Fig. 6A) were performed at different time points after CFA treatment. Overall, we found a significant alleviation of mechanical hyperalgesia after dorsal column activation of Aβ-LTMRs. Specifically, a significantly reversal of the PWT were observed at 2 hours, 7 days, 14 days post-CFA (2 hour: 0.13 ± 0.026 g (pre-stimulation), 0.618 ± 0.069 g (5 min), $p < 0.0001$; 0.633 ± 0.077 g (30 min), $p < 0.0001$) (Figure 6Fi); (day 7: 0.008 ± 0 g (prestim), 0.458 ± 0.062 g, (5 min), $p = 0.0082$; 0.649 ± 0.091 g (30 min), $p = 0.0093$) (Figure 6Fii); (day 14: 0.026 ± 0.006 g (prestim), 0.663 ± 0.094 g (5 min), $p = 0.011$; 0.676 ± 0.089 g (30 min), $p = 0.0079$) (Figure 6Fiii). At days 21 post-CFA, as mechanical hyperalgesia started to recover, no significant change of PWT was observed (Figure 6Fiv-). These results provide direct evidence to support that global activation of Aβ-LTMRs could attenuate mechanical hyperalgesia in chronic pain.

Discussion

In this study, we combined intersectional mouse genetics, opto-tagged electrophysiology recordings, and high-speed imaging behavioral assays to clarify roles of Aβ-LTMRs in transmitting and alleviating mechanical

hyperalgesia. Our results revealed that both global ablation and local activation of Aβ-LTMRs promoted mechanical hyperalgesia, whereas their global activation alleviated it. Therefore, we propose a new model (Figure 7), which integrates the inter-modal crosstalk between the nociceptive pathway and Aβ-LTMRs and the inter-somatotopic crosstalk among Aβ-LTMRs at different spinal segments, to explain the complicated phenotypes of Aβ-LTMRs in mechanical hyperalgesia. Our model suggests that the global activation plus local inhibition of Aβ-LTMRs would be an effective strategy for treating mechanical hyperalgesia.

Complicated function of Aβ-LTMRs in chronic pain

A half century after the introduction of Gate Control Theory (Melzack and Wall, 1965), the exact functions of Aβ mechanoreceptors in chronic pain are still not fully resolved. The primary function of these afferents is mediating discriminative touch and tactile/vibration sensation. However, these neurons also play important roles in “gating” or inhibiting other somatosensory pathways to generate the appropriate sensation. The fast conduction velocity of Aβ-LTMRs put them in a great position for this role. In response to a mechanical stimulus, signals of Aβ-LTMRs arrive at the dorsal spinal cord first and “set up” the “gate” for other mechanosensory pathways with slower conduction velocities (Aδ- and C-LTMRs and high-threshold mechanoreceptors). Thus, activating Aβ-LTMRs has been a commonly sorted

strategy for treating chronic pain (Caylor et al., 2019; Gibson et al., 2019). On the other hand, multiple studies also suggest that Aβ-LTMRs mediate mechanical allodynia in chronic pain conditions (Campbell et al., 1988; Devor, 2009; Dhandapani et al., 2018; Koltzenburg et al., 1992; Liu et al., 2000; Xu et al., 2015). How to consolidate these experimental results?

Here we utilized intersectional genetics to selectively ablate Aβ-LTMRs or optogenetically activate them either locally at the affected site (peripheral) or globally at the dorsal column (central) and examined behavioral outcomes in baseline and chronic pain conditions. Interestingly, activities of locally affected Aβ-LTMR$_S$ in chronic inflammation triggered nociception (Fig. 4), whereas global activities of Aβ-LTMR$_S$, many of which were unaffected, could still inhibit transmission of mechanical pain in both acute and chronic pain conditions in a modality-specific manner (Fig. 3 & 6). This clear distinction of “local” vs “global” functions of Aβ-LTMR$_S$ in mechanical pain transmission, as explained by our model (Figure 7), will help to consolidate the existing data in this topic and provide a theoretic reference for the design of new treatment strategies.

Our findings are somewhat different from two previous studies in this topic but using different genetic tools for ablation or optogenetic activation (Dhandapani et al., 2018, Chamessian et al., 2019). The first study found that DTA ablation

of Trkb+ Aβ-LTMRs attenuates mechanical allodynia in a neuropathic pain (SNI) but not inflammatory pain (CFA) models (Dhandapani et al., 2018). A main difference between ours and this study is the genetic tools, which manipulated largely non-overlapping sensory afferents. We used *Split-Cre* allele that preferentially labeled Aβ-LTMRs in both glabrous and hairy skin, whereas the other study used *TrkB-CreERT2* mice, which preferentially label Aδ-LTMRs (D-hair) in the hairy skin and a few Aβ-LTMRs in the glabrous skin. Here we found that a high percentage (~75%) of paw Meissner corpuscles were innervated by *Split-Cre* labeled afferents (Figs. 1, 2, S1, S2), ~80% these innervation was lost in the ablated mice (Fig. 2), and obvious deficits of DTA-ablated mice in dynamic gentle mechanical force and tactile sensation (Fig. 3). In contrast, the other study showed almost no Meissner corpuscle innervation and found no mechanosensory deficits from paws of ablated mice at the baseline condition. Thus, global DTA ablation using TrkB-CreERT2 and Split-Cre lines would disrupt largely different populations of sensory afferents and thus generated different behavioral outcomes. The second study used a VGlut1-Cre mouse line, which should cover most Aβ-LTMRs, but failed to detect behavior changes when optogenetically activating VGlut1^{Cre}-Aβ-LTMRs in a neuropathic pain model (Chamessian et al., 2019). As the authors discussed in that paper, it is hard to differentiate between touch-like and pain-like pain reflex behaviors without a high-speed camera. This is what we used in this study, which improved resolution of behavior assays.

Targeting Aβ-LTMRs for treating mechanical hyperalgesia and chronic pain

Multiple existing techniques, presumed to involve the manipulation of Aβ-LTMRs, are used in practice for treating chronic pain. The best known one is the SCS, which was developed based on the “gate control theory” and was designed to target Aβ-LTMR axons projecting through the dorsal column (Shealy et al., 1967). The SCS is effective for treating different chronic pain conditions, refractory chronic pain, and even those failed available pharmacological approaches (Gilbert et al., 2022; Sun et al., 2022). Since several types of axons, besides those of Aβ-LTMRs, project through the dorsal column, and can simultaneously be activated by SCS, whether stimulating Aβ-LTMR axons alone in the dorsal column is sufficient for alleviating chronic pain has remained untested. Our study provides direct supportive evidence for the chronic pain-alleviating effect of activating Aβ-LTMRs at the dorsal column (Fig. 6). Our results do not exclude the potential contribution from other dorsal column fibers in this regard. Some Transcutaneous Electrical Nerve Stimulation (TENS) strategies aim to target peripheral Aβ-LTMRs 2-3 dermatomes away from the injury site. Several human trials support the effect of the technique in alleviating pain (Celik et al., 2013; Gardner et al., 2014; Jin et al., 2010; Vance et al., 2012). These practices and effects also align well with our results and model. Finally, our model proposes a potentially more

effective compound strategy to target Aβ-LTMRs for treating mechanical hyperalgesia and chronic pain: activating them globally or 3-4 dermatomes away from the injury site in combination with local inhibition of the affected Aβ-LTMRs.

Acknowledgements

We thank Drs. Sotatsu Tonomura and Ryan Vaden from the Gu lab for their help in electrophysiological experiments. We thank Dr. David Ginty for sharing *Split*^{Cre} and *Advillin*^{FlpO} mouse lines. We thank Dr. Martyn Goulding for sharing the *Tau*$^{ds\text{-}DTRf/f}$*;Ai9*$^{tdTomatof/f}$ mouse line. We thank the previous and current lab members in Gu, Luo, and Ma labs for their help and insightful suggestions. This work is supported by NIH grants NS109059 and DE018661 to J.G.G., and NS083702 to W.L.

Author Contributions

Conceptualization, M.G., J.G.G., and W.L.; Methodology, M.G., A.Y., A.I.Y., J.G.G., and W.L.; Investigation, M.G., A.Y., A.I.Y., P.D., K.K., Q.W., and J.L.; Writing-Original Draft, M.G., and W.L.; Writing – Review & Editing, M.G., P.D., K.K. H.Y., M.M., J.G.G., and W.L; Funding Acquisition, J.G.G. and W.L.; Resources, M.M., J.G.G., and W.L.; Supervision, M.M., J.G.G., and W.L.

Declaration of Interests

The authors declare no competing interests.

Figure Legends

Figure 1. Histological and electrophysiological characterizations of *Split^{Cre}-ReaChR* mice confirmed that *Split^{Cre}* preferentially recombined in Aβ-LTMRs.

(A) Triple immunostaining of a lumbar DRG section showing little overlap between GFP (ReaChR)$^{+}$ DRG neurons and nociceptor markers CGRP or IB4. Scale bars are 50 μm in the figures, otherwise marked.

(B & C) Double immunostaining of DRG sections showing high overlaps between GFP (ReaChR)$^{+}$ DRG neurons and NF200 or RET. White arrows indicate some overlapped neurons.

(D) Double immunostaining of a DRG section showing some overlaps between GFP (ReaChR)$^{+}$ DRG neurons and a proprioceptive marker PV.

(E) Quantification of the percentage of GFP^+ neurons expressing different markers. 6-8 sections/mouse, n = 4-6 mice. Error bars represent Mean ± S.E.M.

(F) Triple immunostaining of a lumbar spinal cord section showing laminar segregation of GFP^+ central terminals and $CGRP^+$ or $IB4^+$ nociceptor terminals.

(G) Double immunostaining of lumbar spinal cord section showing GFP^+ central terminals innervate deeper dorsal horn lamina (III-V), indicated by $VGlut1^+$ staining.

(H-J) Double immunostaining of plantar skin sections showing that GFP^+ peripheral axons are $NF200^+$ and innervate Meissner's corpuscles (revealed by S100 staining) but not $K8^+$ Merkel cells. White arrows indicate some Meissner's corpuscles, while white arrowheads indicate Merkel cells. 6-8 sections/mouse, n = 4-6 mice.

(K) Image showing two $ReaChR/YFP^+$ fibers in an ex-vivo saphenous nerve preparation, one fiber had a node of Ranvier (NR) where patch-clamp recording was made to record action potential (AP) impulses. The asterisk indicates the shadow of the recording electrode tip.

(L) Sample trace showing AP impulse recorded from a $ReaChR/YFP^+$ fiber. The AP impulse was evoked by an electrical stimulus at a distal site of the

saphenous nerve. A stimulation artifact (Stim.) is shown prior to the AP impulse.

(M) Summary data of conduction velocities of AP impulses in ReaChR/YFP$^+$ fibers propagated from the stimulation sites to the recording sites (n = 17).

(N) Diagram illustrating pressure-clamped single-fiber recordings of AP impulses evoked by LED light stimulation and mechanic indentation at the same receptive field in an *ex-vivo* hind paw skin-nerve preparation.

(O) Top panel, sample trace showing an AP impulse evoked by LED light in a receptive field of the hairy skin of the skin-nerve preparation. Middle panel, no AP impulse could be evoked by light stimulation at saphenous nerve bundle. Bottom panel, LED light pulse.

(P-Q) The representative traces showing rapidly adapting (RA, P) and slowly adaptive (SA, Q) AP impulses evoked by mechanical indentation (30 mN) at two different receptive fields where LED lights also evoked AP impulses (red traces at an expanded time scale). The black traces in P and Q after the red traces are mechanically evoked AP impulses at an expanded time scale. Glabrous skin-tibia nerve preparation was used in (P), hairy skin-saphenous nerve preparation was used in (Q).

(R) Numbers of light-sensitive RA (Grey bar) and light-sensitive SA units (Black bar) recorded from the hairy/H (n = 7) and the glabrous skin/G (n = 9).

(S) Mechanical stimulation-response curves of light-sensitive RA and light-sensitive SA units. SA; n = 4 except n = 3 at 80 mN. RA; n = 12.

(T) Mechanical thresholds of light sensitive RA (n = 11) and SA units (n = 4).

Figure 2. Pharmacogenetic ablation of Split^{Cre}-Aβ-LTMRs.

(A) Illustration showing the intersectional genetic strategy to generate *Split^{Cre}-Aβ TauDTR* quadruple mice for specifically ablating Split^{Cre}-Aβ-LTMRs and the protocol timeline.

(B-C) Whole-mount images of lumbar DRGs of vehicle or DTA treated quadruple mice.

(D) Quantification of the tdTomato^{+} neurons per DRG showed a significant decrease in number of tdTomato^{+} DRG neurons with DTA treatment ($p < 0.0001$). The data were normalized to the average number of Tdt^{+} DRG neurons/DRG of control mice. 2-4 DRGs / mouse, n = 5 mice.

(E-F) Images showing tdTomato^{+} central terminals in the dorsal horn of the lumbar spinal cord of vehicle or DTA treated mice. Dotted white area indicates the deep dorsal horn (laminae III-V).

(G) Quantification of the mean tdTomato^{+} fluorescence intensity in the deep dorsal horn showed a significant decrease with DTA treatment ($p = 0.0079$).

The data were normalized to the average mean intensity of Tdt^+ central terminals of control mice. 6-8 sections per mouse, n = 5 mice.

(H-I) Images showing $tdTomato^+$ nerve fibers in the plantar skin of vehicle or DTA treated mice. White arrowheads indicate Meissner's corpuscle innervating fibers in vehicle-treated mice, and white arrow points to a remaining $tdTomato^+$ fiber in the dermis of DTA-treated mice.

(J) Quantification of the number of $tdTomato^+$ fibers innervating Meissner's corpuscles per footpad section showed a significant decrease with DTA treatment ($p = 0.0022$). The data were normalized to the average number of $Tdtomato^+$ fibers innervating Meissner's corpuscles of control mice. 5-7 sections per mouse, n = 6 mice. Error bars represent Mean ± S.E.M. Unpaired, two-tailed Mann-Whitney test. *$p < 0.05$, **$p < 0.01$; ***$p < 0.001$, ****$p < 0.0001$ ns = non-significant.

Figure 3. Ablation of $Split^{Cre}$-Aβ-LTMRs reduced gentle touch sensation but increased mechanical nociception in the glabrous skin.

(A) Illustration showing cutaneous sensory afferents of the ablated plantar skin; green fibers represent nociceptive C and Aδ fibers; red fibers represent RA Aβ-LTMRs innervating Meissner's corpuscles (red capsules) in the dermal papilla; black fibers represent, SA Aβ-LTMRs innervating Merkel cells (black bead-like structures) at the base of dermal papilla; 'X' symbol represents the

DTA-induced selective ablation of RA Aβ-LTMRs in the glabrous skin of DTA-treated *Split^{Cre}-Aβ TauDTR* mice.

(B) Ablation of Split^{Cre}-Aβ-LTMRs did not affect the static mechanosensitivity measured by 50% PWT of the von Frey hair test ($p > 0.99$), n = 9 mice in each group.

(C) Dynamic gentle touch sensitivity, measured by the percentage of paw lifting responses to dynamic cotton swab at the plantar surface, was significantly attenuated in the ablated mice ($p = 0.0014$), 5 trials/mouse, n = 9 mice in each group.

(D) The tape removal time, which inversely reflects the gentle touch sensitivity, significantly increased in the ablated mice ($p = 0.0063$), n = 10 mice in each group. Also see supplementary video 1.

(E) Discriminative touch sensation, indicated by chamber preference of different floor texture, was altered in the ablated mice. Compared to vehicle-treated mice, which show no significant preference for the floor textures ($p = 0.505$), the ablated mice preferred to stay in the loop (smooth) surface compartment over the hook (rough) floor compartment ($p = 0.001$), n = 8 for control and 7 for the ablated mice.

(F) Mechanical pain sensation, indicated by the number of licking episodes with the application of an alligator clip at the plantar skin (1 minute total),

significantly increased in the ablated mice ($p = 0.0002$), n = 10 mice in each group. Also see supplementary video 2.

(G) The ablated mice showed significantly increased mechanical nociception, indicated by 50% PWT, in chronic inflammation condition. The PWT significantly decreased in ablated mice at 2 hour ($p = 0.0149$), 14th day ($p = 0.0427$), 21st day ($p = 0.0012$), and 28th day ($p = 0.0012$ g) in comparison to vehicle-treated mice. n = 9 mice per group except the days 21 and 28 (vehicle: n = 7 mice and DTA: n = 6 mice). Blue arrow indicates the time of intraplantar injection of CFA.

(H) The ablated mice showed no significant change in thermal hyperalgesia, indicated by the paw withdrawal latency (PWL) of the Hargreaves test, in chronic inflammation condition. Error bars represent Mean ± S.E.M. Unpaired, two-tailed Mann-Whitney test. *$p < 0.05$, **$p < 0.01$; ***$p < 0.001$, ns = non-significant.

Figure 4. Local optogenetic activation of Split^{Cre}-Aβ-LTMRs evoked nociception in both chronic inflammatory and neuropathic pain conditions.

(A) Illustration showing peripheral optogenetic activation of Split^{Cre}-Aβ-LTMRs in the plantar (glabrous) skin by a blue laser (473 nm).

(B) The percentage of paw withdrawal response increased in an intensity-dependent manner.

(C) Paw withdrawal latency decreased in an intensity-dependent manner.

(D) Pain scores of mouse behaviors triggered by blue laser at different intensities at the baseline condition. Also see supplementary video 4.

(E) Compared to the baseline condition, 5 mW blue laser triggered significantly higher percentages of paw withdrawal response in CFA-induced inflammatory pain model at 2 hour ($p = 0.044$), days 1 ($p < 0.0009$), 3 ($p < 0.007$), 7 ($p = 0.0009$), 14 ($p < 0.0001$), 21 ($p = 0.0009$), and 28 ($p = 0.0003$).

(F) Compared to the baseline condition, the PWLs in response to 5 mW blue laser significantly decreased at days 3 ($p = 0.0015$), 7 ($p = 0.0005$), and 14 ($p < 0.0001$). Non-significant changes were observed at 2 hour ($p = 0.365$), days 1 ($p = 0.06$), 21 ($p = 0.09$), and 28 ($p = 0.254$). n = 9 mice in each group (D-F).

(G) Compared to the baseline condition, 5 mW blue laser triggered significantly higher pain scores at 2h ($p = 0.037$), days 1 ($p = 0.0022$), 3 ($p = 0.05$), 7 ($p < 0.0001$), 14 ($p = 0.0005$), 21 ($p = 0.018$), and 28 ($p = 0.017$). Kruskal-Wallis test. Also see supplementary video 5.

(H) Timeline and illustration of the conditioned place-preference paradigm.

(I) CFA-treated Split^{Cre}-ReaChR mice showed significantly higher percentage of aversion in comparison to the saline treatment, n = 7 in saline and n = 6 in

CFA groups ($p = 0.004$). Compared to the baseline condition, 5 mW blue laser triggered significantly higher percentages of paw withdrawal response in a MPNL-induced neuropathic pain model at days 1 ($p = 0.0112$), 3 ($p < 0.0001$), 7 ($p < 0.0001$), 14 ($p < 0.0001$), 21 ($p < 0.0001$) and 28 ($p < 0.0001$).

(J) Compared to the baseline condition, the PWLs in response to 5 mW blue laser significantly decreased at days 7 ($p = 0.0241$), 14 ($p = 0.0032$), 21 ($p = 0.0024$) and 28 ($p = 0.0022$). Non-significant changes were observed at days 1 ($p = 0.835$), and 3 ($p = 0.224$). n = 7 mice in each group (G-I).

(K) Compared to the baseline condition, 5 mW blue laser triggered significantly higher pain scores at days 1 ($p = 0.0292$), 3 ($p < 0.0001$), 7 ($p < 0.0001$), 14 ($p < 0.0001$), 21 ($p < 0.0001$) and 28 ($p < 0.0001$).

Error bars represent Mean ± S.E.M. One way ANOVA followed by Tukey's multiple comparison test except the panel E. *$p < 0.05$, **$p < 0.01$, ***$p < 0.001$, ****$p < 0.0001$.

Figure 5. Split^{Cre}-ReaChR^{+} Aβ-LTMRs in the hind paw glabrous skin fire more action potentials in response to mechanical forces after CFA treatment.

(A) Two sample traces showing mechanically evoked RA impulses recorded from light sensitive (ReaChR/YFP tagged) afferent fibers that innervate the

glabrous skin of hind paws. Top, saline-injected paw (control), Bottom, CFA-injected paw. RA impulses were evoked by tissue indentation at 30 mN at the receptive field where red LED light evoked impulses. Sample traces at expanded time scale show light-evoked (red) and mechanically evoked AP impulses (black).

(B) Summary data of RA impulses evoked by tissue indentation at 0, 15, 30, and 80 mN in light-sensitive afferent fibers of saline-injected group (n = 7) and CFA-injected group (n = 5). Two-way ANOVA with post hoc Bonferroni's test, * $p < 0.05$, *** $p < 0.001$.

(C) Similar to (A) except SA impulses were recorded from a saline-injected paw (top) and CFA-injected paw (bottom).

(D) Similar to (B) except SA impulses were recorded from saline-injected group (n = 1) and CFA-injected group (n = 6).

(E) Percent of light-sensitive afferent fibers that show RA (n = 7) or SA impulses (n = 1) in saline group, and RA (n = 5) or SA impulses (n = 6) in CFA group, Chi's square test * $p < 0.05$.

(F) Thresholds of RA-LTMRs in control (n = 7) and CFA (n = 5) groups.

(G) Thresholds of SA-LTMRs in control (n = 1) and CFA (n = 6) groups.

In B, D, F, and G, data represent Mean ± SEM.

Figure 6. Dorsal column activation of Split^{Cre}-ReaChR^{+} Aβ-LTMRs alleviated mechanical hyperalgesia in the chronic inflammatory pain model.

(A) Illustration showing our experimental paradigm: a light-cannula implanted above the dorsal column at the T11 segment of the spinal cord. The inset region is zoomed in to show that blue laser stimulates ascending axons of Split^{Cre}- ReaChR^{+} Aβ-LTMRs (green color) projecting through the dorsal horn. VFH tests were performed at the baseline and different time points of the CFA-induced inflammatory pain model.

(B) Spinal cord stimulation using 0.5 mW blue laser did not significantly change the PWT (5 mW: prestim. vs 5 min., 30 min., 90 min., 120 min., $p > 0.99$ at all-time points; 10 mW: prestim. vs 5 min., $p < 0.0001$; 30 min., $p = 0.048$; 90 min., 120 min, p = ns). n = 7 mice. Error bar: Mean ± SEM. Two-way ANOVA followed by Bonferroni multiple comparison test. *$p < 0.05$, ****$p < 0.0001$.(C) Quantification of c-Fos+ neurons in the superficial and deep dorsal horn laminae of the thoracic and lumbar spinal cord of no-light and light-stimulated Split^{Cre}-Aβ ReaChR mice (without treatment). A significant increase in the number of c-Fos+ neurons was found in deeper layers after light stimulation (Thoracic: No light vs Light, $p < 0.0001$; Lumbar: No light vs Light, $p < 0.0001$).

(D)Triple RNAScope *insitu* hybridization staining of lower thoracic spinal cord section showing most c-Fos^{+} neurons in deeper dorsal horn laminae (III-V) are inhibitory interneurons indicated by an overlap with VGAT^{+} staining.

(E) Quantification of excitatory (VGLUT2^{+}) and inhibitory (VGAT^{+}) interneurons co- labelled with c-Fos in the superficial and deep dorsal horn laminae of the thoracic and lumbar spinal cord after light stimulation in Split^{Cre}-Aβ ReaChR mice (without treatment).

(F) Global activation of Split^{Cre}-ReaChR^{+} Aβ-LTMRs alleviated mechanical hyperalgesia in mice with CFA-induced chronic inflammatory pain. i. Spinal stimulation at 2 hour post-CFA significantly reversed the PWT at 5 min (prestim. vs 5 min., $p < 0.0001$) and 30 min ($p < 0.0001$) post-light stimulation.

ii. At D7 post-CFA, a significant reversal of PWT was observed at 5 min. (prestim. vs 5 min., $p = 0.0082$) and 30 min. ($p = 0.0093$) post-light stimulation.

iv. At D14 post-CFA, a significant reversal of PWT was observed at 5 min (prestim. vs 5 min., $p = 0.011$) and 30 min. ($p = 0.0079$) post-light stimulation.

v. At D21 post-CFA, no significant change of PWT was observed after spinal light stimulation. n = 6 mice except panel C (3 mice, 5-7 sections per mouse for statistical comparison) and E (3 mice, 3-4 sections per mouse). Error bars represent Mean ± S.E.M. Two-way ANOVA followed by Bonferroni test except the panel C & E (Mann-Whitney test). *$p < 0.05$, **$p < 0.01$, ****$p < 0.0001$, ns = non-significant.

Figure 7. A model to explain how Aβ-LTMRs function in both transmitting and alleviating mechanic hyperalgesia.

Illustration shows anatomy of central projections of nociceptors and Aβ-LTMRs and the inter-modal and inter-somatotopic crosstalk. Central terminals of nociceptors only innervate one or two spinal cord segments, whereas Aβ-LTMRs have ascending and descending axons projecting through the dorsal column and 3rd order collaterals covering the dorsal horn of 6 to 8 spinal cord segments. This anatomical feature allows an Aβ-LTMR to interact with nociceptors and other Aβ-LTMRs in 3 to 4 dermatomes away.

STAR * Methods

Key resource table

REAGENT or RESOURCE	SOURCE	IDENTIFIER
Antibodies		
Chicken polyclonal anti-GFP	Aves Labs	Cat# GFP-1020; RRID:AB_10000240
Rabbit polyclonal anti-GFP	Invitrogen	Cat# A-11122; RRID:AB_221569
Rabbit polyclonal anti-CGRP	ImmunoStar	Cat# 24112; RRID:AB_572217

Rabbit polyclonal anti-NF200	Sigma-Aldrich	Cat# N4142; RRID:AB_477272
Chicken polyclonal anti-NF200	Aves Labs	Cat# NFH-3-1003; RRID:AB_2313552
Guinea pig polyclonal anti-VGLUT1	Millipore	Cat# AB5905; RRID:AB_2301751
Rabbit polyclonal anti-S100	Abcam	Cat# ab34686; RRID:AB_777793
Rat anti-K8 (Troma-1)	Univ of Iowa/DSHB	N/A
Rabbit anti-Parvalbumin	Swant	Cat# PV27; RRID:AB_2631173
Rabbit monoclonal anti-Ret	Immuno-Biological Laboratories	Cat# 18121; RRID:AB_2301042
Rabbit polyclonal anti-DsRed	Takara Bio	Cat# 632496; RRID:AB_10013483
Rabbit monoclonal anti-c-Fos	Cell Signaling Technology	Cat# 2250; RRID:AB_2247211
IB4, Alexa Fluor 488 conjugate	Invitrogen	Cat# I21411; RRID:AB_2314662
IB4, Alexa Fluor 594 conjugate	Invitrogen	Cat# I21413;

		RRID:AB_2313921
Goat anti-rabbit IgG (H+L), Alexa Fluor 488	Thermo Fisher Scientific	Cat# A-11008; RRID:AB_143165
Goat anti-rabbit IgG (H+L), Alexa Fluor 594	Thermo Fisher Scientific	Cat# A-11012; RRID:AB_2534079
Goat anti-rabbit IgG (H+L), Alexa Fluor 647	Thermo Fisher Scientific	Cat# A-21244; RRID:AB_2535812
Goat anti-rabbit Cy3	Thermo Fisher Scientific	Cat# A10520, RRID:AB_2534029
Chemicals		
Diphtheria Toxin	Sigma-Aldrich	Cat# D0564
CFA	Sigma-Aldrich	Cat# F5881
TritonX-100	Sigma	Cat# T8787
OCT compound	Thermo Fisher Scientific	Cat# 23-730-571
DMSO	Sigma-Aldrich	Cat# 472301
Benzyl Alcohol	Sigma-Aldrich	Cat# 8.22259
Benzyl Benzoate	Sigma-Aldrich	Cat# B9550
Glycerol	Invitrogen	Cat# 2130
Normal goat serum	Jackson Immuno Research	Cat# 005-000-121
Critical commercial assays		

RNAScope probe: cFos	ACD	Cat# 316921
RNAScope probe: Slc17a6	ACD	Cat# 319171
RNAScope probe: Slc32a1	ACD	Cat# 319191
RNAscope™ Multiplex Fluorescent Detection Kit v2	ACD	Cat# 323110
RNAScope™ H_20_2 and Protease Reagents	ACD	Cat# 322381
TSA Plus Cyanine 3 System	AKOYA BIOSCIENCES	Cat# NEL744001KT
Experimental models		
Advillin^{FlpO}	Dr. David Ginty	N/A
Split^{Cre}	Dr. David Ginty	N/A
Rosa^{ReaChR}	Jackson Laboratory (USA)	JAX: #024846
Tau$^{ds\text{-}DTRf/f}$	Dr. Martin Goulding	N/A
Ai9$^{tdTomatof/f}$	Jackson Laboratory (USA)	JAX: #007905
C57BL/6J	Jackson Laboratory (USA)	JAX: #000664
Software and Algorithms		
FASTCAM Viewer 4	Photron	N/A

Prism 9	GraphPad	RRID:SCR_002798
Fiji	NIH	RRID:SCR_002285
Illustrator	Adobe	RRID:SCR_014198
BioRender	BioRender	RRID:SCR_018361
ANY-Maze	Stoelting Co.	RRID:SCR_014289
Other		
FASTCAM Mini UX100	Photron	N/A
Zoom Wide Angle Telephoto 24-85mm f2.8	Nikon	N/A
473 nm blue laser	Shanghai Laser and Optics Century	Cat# BL473T8-150FC
Hp 15MHZ Function Waveform Generator	Hewlett Packard	Part# 33210A
von Frey filaments	Stoelting	Cat# 58011
Perforated wire mesh platform	Ugo Basile	Part #37450-045
Hargreaves apparatus	UCSD Instruments	N/A
Hot plate analgesia meter	IITC Life Science	Cat# 39
Pigtail Rotary Joint, 200 µm, 0.39 NA Fiber, FCPC, 1.25 Ferrule	ThorLabs	RJPFL2

Digital Optical Power Meter	ThorLabs	PM100A
Photodiode Power Sensor	ThorLabs	S120C
Light cannula	ThorLabs	CFMXB05
Velcro® Tape	Velcro	Part# 90197
Krazy®Glue	Krazy Glue	Part #963257

RESOURCE AVAILABILITY

Lead contact

For information and requests related to electrophysiological recordings of this manuscript, please contact Dr. Jianguo Gu (jianguogu@uabmc.edu). For inquiries related to other results and experiments in this manuscript, please contact Dr. Wenqin Luo (luow@pennmedicine.upenn.edu).

Data and code availability

- This paper does not report original code.
- Any additional information required to reanalyze the data reported in this paper is available from the lead contact upon request.

MOUSE MODELS

Advil^{FlpO} (Choi et al., 2020) and *Split*^{Cre} (Cui et al., 2016; Rutlin et al., 2014) mice were imported from Dr. David Ginty's lab at the Harvard University, and the *Tau*^{dsDTR} (Duan et al., 2014) mouse line was imported from Dr. Martyn

Goulding's lab at the Scripp's institute. Other mice (*Rosa*^{ReaChR}, strain #:024846; Ai9, strain #:007905, and C57BL/6J, strain #:000664) were purchased from Jackson's laboratory. Animals were housed in facilities at the University of Pennsylvania and at the University of Alabama at Birmingham. All experiments were conducted in accordance with the National Institute of Health guidelines and with approval from the Institutional Animal Care and Use Committee of University of Pennsylvania and University of Alabama at Birmingham. Adult male and female mice of desired genotypes were kept in a standard 12-h light/dark cycle, with water and food pellets available *ad libitum*.

Method details

Immunohistochemistry of cryosections

Mice were anesthetized using Ketamine/xylazine/acepromazine cocktail and transcardially perfused with 4% PFA in phosphate buffer solution (PBS). Lumbar spinal columns, DRGs, and skin pieces were dissected and post-fixed for 2-4 hours in 4% PFA in PBS at 4°C, cryoprotected in 30% sucrose in PBS O/N at 4°C, and embedded in OCT. 20 µm cryosections of spinal cord, DRG and skin were cut using a cryostat (Leica CM1950). DRG sections were collected on Superfrost™ Plus slides (Fisherbrand) and allowed to dry at room temperature overnight, while spinal cord and skin sections were collected in multi-well plate and 1.5mL Eppendorf tubes (Skin sections) for floating section immunostaining. Slides or floating sections were washed in PBS containing 0.2%

TritonX-100 (3X 10 minutes) and then blocked in PBS containing 5% lamb serum and 0.2% TritonX-100 (PBT) for 1 hour at room temperature. Primary antibodies were diluted in the same buffer, incubated O/N at 4°C, and then washed in PBT (3x10 minutes). Secondary antibodies were incubated in blocking buffer at 1:500 dilution for one hour at room temperature. Slides or floating sections were then washed in PBT (3x10 minutes), mounted with Fluormount and cover-slip, and sealed using clear nail-polish. Primary antibodies used include chicken anti-GFP (1:1000; Aves, GFP-1020), rabbit anti-CGRP (1:1000; Immunostar, 24112), rabbit anti-NF200 (1:1000; Sigma, N4142), chicken anti-NF200 (1:1000, Aves labs, NFH-3-1003), guinea pig anti-VGlut1(1:1000; Millipore, AB5905), rat anti-K8 (Troma-1) (1:100; Univ of Iowa/DSHB), rabbit anti-Ret (1:100, Immuno-Biological Laboratories, 18121), rabbit anti-parvalbumin (1:200, Swant, PV27), rabbit anti-S100 (1:200, Abcam, ab34686), rabbit anti-cFos (1:800; Cell Signaling Technology, 2250), and Alexa 488 or 594 conjugated IB4 (1:500; Invitrogen, I21411). Secondary antibodies used are Alexa 488, Alexa 594, Cyan or Alexa 647 conjugated goat anti-rabbit antibody, Alexa 647 conjugated goat anti-chicken antibody, and Alexa 647 conjugated goat anti-guinea pig antibody. Secondary antibodies were purchased from either Invitrogen or the Jackson Immunoresearch.

Dissection and clearing of whole mount DRGs

After anesthetization and transcardiac perfusion, L4/L5 DRGs of mice with desired genotypes were dissected and collected in 1.5 mL Eppendorf tubes, followed by three washings with 1X PBS for 15 min, and then cleared by 50% glycerol/PBS (20 minutes at room temperature) and 75% glycerol/PBS (for 10-20 more minutes). DRGs were mounted in 75% glycerol for imaging.

Whole mount immunostaining of skin samples

Mice were anesthetized and transcardially perfused using 4% PFA. Electric trimmer was used to remove excess of the hair from different body parts. Commercial hair remover (NAIR™) was applied to the skin to remove the remaining hair. Tape-striping using lab-tape and Kimwipes™ was performed until the skin glistered. Skin samples at different body regions, ~3 cm^2 size, were then dissected out and rinsed with PBS 2-3 times for 5 minutes. Each skin piece was further cut into small pieces. The skin samples were fixed for another 2-3 h in 4% PFA/PBS at 4ºC, and any excess fat and hair were removed followed by three times PBS rinses at room temperature. Washing was done every 30 minutes for at least 4-5 hours with PBST (0.5% TX100) at room temperature. Primary antibodies (Chicken anti- NF200 Heavy (Aves Labs) 1:500, Rabbit anti-S100 (Abcam) 1:500, Rabbit anti-NF200 (Sigma) 1:1000, Rabbit anti-GFP (Invitrogen) 1:1000, Rabbit anti-DsRed (Clontech) 1:500, Rat anti-K8 or TROMA-1 (DSHB) 1:100) in chilled blocking solution (5% heat inactivated goat serum, 75% PBST, 20% DMSO) were applied and incubated

on rocker at room temperature for 72 hrs. Tissues were rinsed in PBST for 3 times followed by a 30-minute wash for at least 4-5 hours with PBST. Tissues were then incubated in secondary antibody in blocking solution at RT for 48 hrs. PBST was used to rinse the tissues for 3 times followed by a wash every 30 minutes for at least 4-5 hours with PBST. Tissues were dehydrated (1-2 hrs for each) in serial MeOH (Methanol)/PBS dilutions (25, 50, 80, 100) rocking at RT. Tissue was kept in 1:1 MeOH:BABB (1 part Benzyl Alcohol: 2 parts Benzyl Benzoate) solution in 10 mL glass vial for 1-3 hrs rocking at room temperature. Tissue was cleared in 100% BABB and mounted on a slide (with little BABB). Four drops of grease were put at four corners around the tissue and a cover glass was put over it with gentle pressure so that the coverslip sticks with the mounting tissue/grease.

RNAScope *in situ* hybridization

Intact spinal columns were dissected from CO_2 euthanized mice and rapidly frozen in OCT on a dry-ice/ethanol bath. Using a cryostat, 20 µm cryosections were collected on Superfrost Plus slides (Fisher, 22–034-979) and allowed to dry for at least 2 hours at room temperature. RNAScope *in situ* hybridization was performed in accordance with the manufacturer's instructions. RNAScope probes, Mm-cFos (316921-C3), Mm-Slc32a1 (319191), Mm-Slc17a6 (319171-C2), were purchased from ACD (Advanced Cell Diagnostics, Inc.).

Image Acquisition

Images were taken using a Leica SP5II confocal microscope (fluorescent). Image processing and figure generation were performed in Fiji-ImageJ and Adobe Illustrator.

Ex vivo skin-nerve preparation

Split^{Cre}*;Advil*^{FlpO}*;Rosa*$^{ReaChRf/+}$ mice of both male and female sexes were used, and most of them (31 mice) were aged 6 to 15 weeks and 4 were over 20 weeks. In one set of experiments, naïve animals were used, and in another set of experiments, animals were randomly assigned into saline and CFA groups. In saline group, each animal was injected with 10 µl saline into both hind paws. In CFA group, each animal was injected with 10 µl CFA (5 µg/10 µL) into both hind paws. 4-7 days after the injection of saline or CFA, animals were anesthetized with 5% isoflurane and then sacrificed by decapitation. The saphenous nerves with their innervated hairy skin of the hind paws or the tibial nerves with their innervated glabrous skin of the hind paws were dissected out from the animals. The skin-nerve preparation was then placed in a Sylgard Silicone-coated bottom of a 100-mm recording chamber that contained the Krebs bath solution described below. The fat, muscle and connective tissues on the nerves and the skin were carefully removed with a pair of forceps. The skin was affixed to the bottom of the chamber by tissue pins with epidermis side facing down, and the nerve bundle was affixed by a tissue anchor in the same recording chamber. The recording chamber was then mounted on the stage of the Olympus

BX51WI upright microscope. The skin-nerve preparation was superfused with a normal Krebs bath solution that contained (in mM): 117 NaCl, 3.5 KCl, 2.5 $CaCl_2$, 1.2 $MgCl_2$, 1.2 NaH_2PO_4, 25 $NaHCO_3$, and 11 glucose (pH 7.3 and osmolarity 325 mOsm) and was saturated with 95% O_2 and 5% CO_2. The Krebs bath solution in the recording chamber was maintained at 24℃during experiments recordings. To facilitate the pressure-clamped single-fiber recordings, the cutting end of the nerve bundle was briefly exposed to an enzyme solution that contained 0.1% dispase II and 0.1% collagenase in Krebs solution for 30 to 60 s, and the enzyme was then washed off by the continuous perfusion of the normal Krebs solution.

Pressure-clamped single-fiber recordings

The pressure-clamped single-fiber recording was performed in a manner similar to our previous studies (Sonekatsu et al., 2020). In brief, recording electrodes were made by thin-walled borosilicate glass tubing without filament (inner diameter 1.12 mm, outer diameter 1.5 mm). They were fabricated using a P-97 Flaming/Brown Micropipette Puller and fire polished to make tip diameter at 10 to 50 μm. The recording electrode was filled with the Krebs bath solution, mounted onto an electrode holder which was connected to a high-speed pressure-clamp device (ALA Scientific Instruments, Farmingdale, NY). Under a 40x objective, individual nerve fibers in the cutting end of the whisker afferent nerve bundle were separated by a positive pressure of approximately +10

mmHg delivered from the recording electrode. The end parts of nerve fibers in the number of 3 to 30 were then aspirated into the recording electrode by a negative pressure at approximately -10 mmHg. Once the nerve ends reached approximately 10 to 30 μm in length within the recording electrode, the pressure in the recording electrode was readjusted to -5 to -1 mmHg and maintained throughout the experiment. To identify nerve fibers that are ReaChR/YFP^{+}, a beam of red LED light (wave length 617 nm) was focused through the 40x objective to the skin to search the receptive field where action potential impulses could be evoked by the LED light. ReaChR can be activated by blue and orange lights (Lin et al., 2013). In searching the light sensitive receptive field, LED light were continually applied with 5-ms light pulses at the frequency of 0.1 Hz, and the intensity of the LED light was at 4.5 mW. To determine mechanical sensitivity of the light-sensitive receptive field, a mechanical indenter (Aurora scientific: 300C-I) was used to apply mechanical stimulation at the pre-identified light-sensitive receptive field. The tip size (in diameter) of the indenter was 0.3 mm for the hairy skin and 0.8 mm for the glabrous skin. The mechanical stimulation was applied under the force control module in which a ramp-and-hold stepwise force was applied to the skin. Prior to the application of the stepwise force, the tip of the indenter was lowered to the surface of the receptive field with a 1-g force and then the 1-g force was canceled to 0 so that the tip of the indenter was just in contact with the receptive field surface but without having any force applied to the receptive field. The

indenter was connected to a Digidata 1550B Digitizer and the stepwise force was delivered to the indenter using the command from pClamp 11 software. The step force commanders were calibrated by applying indenter at finger tips, paw pads and other areas of plantar skin, and the actual forces applied to these skin areas were measure and used to correct the commander force steps. The actual ramp-and-hold force steps were applied from 0 mN to 5, 30, and 80 mN. The duration of the ramp (dynamic phase) was 10 ms, and the duration of the holding step (static phase) was 0.98 s. The minimal force step at which AP impulses was elicited was defined as mechanical threshold of the receptive field. The signals were recorded using a Multiclamp 700B amplifier and signals were sampled at 25 kHz with band path filter between 0.1Hz and 3 kHz on AC recording mode.

In a different set of experiments, conduction velocity of the ReaChR/YFP-positive saphenous nerves were determined. In this set of experiments, ReaChR/YFP-positive nerves were visualized under a fluorescent microscope and a loose-patch recording was made at the node of Ranvier in a similar manner described in our previous studies (Tonomura et al., 2022). Impulses were evoked at the peripheral end of the saphenous nerve bundle using a suction stimulation electrode. The suction stimulation electrode's tip size was approximately 0.5 mm in diameter and was fire polished. The peripheral end of the saphenous was aspirated into the suction stimulation electrode with a tight fitting by negative pressure. The negative

pressure was continuously applied into the suction stimulation electrode to maintain the tight-fitting during experiments. To initiate AP impulses at the peripheral end of the saphenous nerve, monophasic square wave pulses were generated by an electronic stimulator (Master-8, A.M.P.I, Israel) and delivered via a stimulation isolator (ISO-Flex, A.M.P.I, Israel) to the suction stimulation electrode. The duration of each stimulation pulse was 50 µs and the stimulation intensity for evoking impulses were 100 to 200 µA.

Diphtheria Toxin (DTA) Administration

Either Diphtheria Toxin (20 µg/kg, Sigma-Aldrich, USA) or the water (vehicle) was injected (intraperitoneal) into *Split*^{Cre};*Advil*^{FlpO};*Tau*$^{ds\text{-}DTR\ f/+}$;*Ai9*$^{tdTomato f/+}$ mice at the age of 6-week old for 7 days. Two weeks after the last injection, some mice were sacrificed and perfused. Their tissues (spinal cord, DRGs, and skin) were collected for histological characterization to determine efficiency of DTA-induced ablation. The remaining mice were used for different behavioral tests from one month after the last DTA or vehicle injection.

CFA-induced inflammatory pain model

The CFA-induced inflammatory pain model was generated as previously described (Beattie *et al*., 2022). Briefly, a mouse with the desired genotype was anesthetized by isoflurane, and the plantar surface of one paw was sterilized. 10 µL of CFA emulsion (Sigma, F5881) was slowly injected into the plantar skin

surface (from the lower middle walking footpad at the ventral surface towards the plantar area) using a 0.5 mL insulin syringe. Injection site was hold using gentle thumb pressure to avoid leakage of CFA for ~10 s. The success of model was confirmed by measuring the paw-thickness by a digital electronic caliper (#30087-00, Fine Science Tools) (1 day post injection) and mechanical sensitivity using von Frey filaments.

Medial Plantar Nerve Ligation (MPNL)-induced neuropathic pain model

The MPNL model was generated as previously published (Sant'Anna et al., 2016). Briefly, a mouse with the desired genotype was anesthetized using isoflurane. After sterilizing the paw skin, the medial surface of the ankle of one leg was incised (0.5 cm) using #11 blade to expose the medial plantar nerve. One ligation was performed with a 4–0 catgut suture (Ethicon). The skin was sealed. After waking up, mice were returned into the home cage.

Behavioral Assays

von Frey Hair Assay

To test the static touch sensitivity, mice were habituated for 2 days in the behavioral room. Under Plexiglas chambers (11.5 x 4.5 x 4 cm), they were kept over a perforated wire mesh platform (Ugo Basile, Italy, Part #37450-045) which had 5 x 5 mm gaps, for 1 h before starting the experiment. Paw withdrawal threshold was assessed using the up-down method (Chaplan et al.,

1994) as described previously (Cui et al., 2022). Briefly, 8 calibrated and logarithmically spaced von Frey monofilaments (bending forces: 0.008, 0.02, 0.04, 0.07, 0.16, 0.4, 0.6 and 1 g; Stoelting, Wood Dale, IL) were used. These were applied tangentially to the plantar surface for ~3-4 s with enough force to cause a slight buckling of the filament. First, the middle filament (0.16 g) was applied to the hind paw. If the mouse showed a withdrawal, an incrementally lower filament was applied. If there was no response, an incrementally higher filament was applied. Trials were separated by at least 2-3 minutes to avoid sensitization and learning. A positive response was characterized as a rapid withdrawal of the paw away from the stimulus fiber within 3-4 s (Sudden withdrawal, flicking or licking of the tested paw). Testing was continued until four filaments were applied (heavier or lighter, depending on the exact filament size to which the last response occurred) after the first one that produced a withdrawal. The final value of 50% withdrawal threshold was calculated by using pseudo-log calculator in Excel which uses the following equation (Chaplan et al., 1994):

50% withdrawal threshold (g) = (10[Xf + kd])/10,000

Where Xf = value (in log units) of the final von Frey filament used; k = tabular value for the pattern of positive/negative value and d = mean difference (in log units) between stimuli.

The observer was blind to the genotype and the drug-treatment while performing the behavioral experiments.

Cotton Swab Assay

After performing von Frey testing, on the consequent day, gentle dynamic touch-evoked sensitivity was measured as described previously (Ranade et al., 2014). Mice were placed under transparent Plexiglas chambers on an elevated wire-mesh platform floor. The floor consists of mesh-like grids that are accessible from below due to small gaps of ~5×5 mm. Mice were habituated 1 h daily for 2 days on this setup in the behavior room and allowed to acclimate for 1 hour before testing. A cotton swab from a cotton applicator (Puritan 25-806 1WC) was manually pulled so that it was “puffed out” to ~3X the original size. When the mouse was at rest, a constant sweeping motion from heal towards the toes was used underneath the mouse paw. Mice were recorded using high-speed imaging camera (500 & 1000 fps). Their paw withdrawal response and other spontaneous behaviors were analyzed. Five trials were performed with ~5 minutes interval between each sweep. Both hind paws were used randomly. The videos were saved in an external hard drive and later analyzed for the number of hind paw withdrawals out of 5 times as a percentage (%) response for each mouse and averaged.

Tape Removal Assay

This assay was performed over glabrous skin (plantar surface) of the mice slightly modified from the (Liu et al., 2018). Mouse was habituated in a transparent plexiglas rectangular chamber over an elevated perforated wire-mesh platform for 45 minutes. Mouse was removed from the enclosure,

and a 9.5 mm diameter, red, circular adhesive Microtube Tough-Spots label (RPI 247106R) was attached to the plantar surface of the hind paw. The mouse was returned to the chamber immediately for video recording. The behavior of mice was recorded using a HD web camera (C922 Pro HD Stream Webcam). The time that each mouse took in removing the tape was measured. 5 minute was the cutoff time for the experiment.

Texture-Preference Assay

A chamber with two compartments separated by a smaller mid-compartment was designed. The two big chambers' floors were covered with loop (Soft side) or hook (Rough side) of Velcro tape, respectively. Also, each chambers had distinctive visual cue patterns (white and black stripes vs white checkered duct tapes). Middle chamber separating these two chambers was completely black, and its floor was made to the level of the two other chambers using plane thick white cardboard. Experiment was done in dim light. Daily for 3 days, each mouse was given restricted habituation of 20 minutes in each chamber. On 4th day, each mouse was allowed to move freely in all chambers for 20 minutes and videotaped from the upside. These videos were analyzed using AnyMaze software for quantifying the total time spent in each chamber.

Plantar-pinch Assay

Mice were habituated in a transparent cylindrical glass chamber (Diameter 10 cm) for 30 minutes. An alligator clip (Amazon, "Generic Micro Steel Toothless Alligator Test Clips 5AMP"), which produces 340 g force, was applied to the

ventral skin surface between the footpads. The animals were returned into the chamber, and their behaviors were video recorded using a high-speed imaging camera (80-200 fps) for 60 s. Behaviors, such as licking, wiping, shaking and scratching episodes, were quantified. Those animals with the clip somehow removed before 60 s cutoff were not considered in the study.

Hargreaves Plantar Assay

Mice were placed in opaque rectangular Plexiglas chambers over the glass surface of the Hargreaves apparatus (UCSD Instruments, San Diego, CA, USA), and allowed to acclimate for ~45 minutes. Mice urine or feces, if any, were removed and the hind paw and the glass surface were cleaned and dried using wipes immediately. A thermostat was used to assess the constant temperature of the glass plate (~22°C ± 1). The heat stimulus was applied from a bulb beneath the glass, to the middle of the plantar surface of the hind paw. Either a brisk paw withdrawal (flick) or licking in response to the thermal stimuli was considered as a positive response. Cutoff time was 20 s. Three trials with a gap of 10 minutes were taken and averaged as the paw withdrawal latency (in second).

Open Field Activity Assay

Mice were habituated for two days in the behavior room in their cage for 45 minutes in the dim light condition. On the third day, mouse was directly kept in the center of the arena and the behavior was recorded using a webcam from the upside. The experimenter was not present in the room while recording the

behavior to avoid observer-related behavioral changes. The total recording time was 20 minutes. Before starting experiment in the next mouse, the surface of arena was cleaned using 40% alcohol and allowed to dry for 10 minutes. The videos were analyzed using AnyMaze software to measure the time spent in the Central and peripheral zone as well as the overall distance traveled.

Static Hotplate Assay

For the static hot plate test, mice were placed on top of a hot plate (IITC, Life Science), preset to 50 ± 0.5 °C covered by a transparent plexiglas chamber. The behavior of the mouse was recorded using a high-speed imaging camera (200 fps). Videos were analyzed, and the latency to lick or flick the hind paw or jumping was quantified. Three trials at intervals of at least 15 min were taken and the average score for each mouse was obtained. To avoid tissue injury of the mice, a cutoff of 30 s was set.

Incremental Hot Plate Assay

The incremental hot plate test was carried out on the same apparatus using different settings, with at least 24 h rest from the static hotplate assay. The initial temperature was set to 28 °C and increased by 6 °C / min towards a final temperature of 55 °C (Alshahrani et al., 2012). The temperature when the first hind paw lick occurred was recorded. If no hind paw lick was observed, the test was terminated at 55 °C. Three trials at intervals of at- least 15 min were taken and the average temperature for each mouse was obtained.

Dry-ice Assay

Mice were placed in Plexiglas chambers on a 2.5 mm thick elevated glass plate and allowed to habituate for at least 45 min. When the mouse was completely at rest, a dry ice pellet (1 cm diameter) was applied to the lower glass surface underneath the hind paw of the animal, and the withdrawal (flick, lick, or both) latency was measured using a stopwatch. Each hind paw was tested randomly for three times with at least 15 min interval in between two consecutive trials. To avoid frost-induced tissue injury, the cutoff latency was set to 10 s.

Tape Response Assay

This assay was performed over hairy (back) skin with slight modifications (Dhandapani et al., 2018). Mice were habituated in a transparent Plexiglas rectangular chamber over an elevated perforated wire-mesh platform for 45 minutes. They were removed, and a small piece of laboratory tape (~3 cm × 1 cm) was placed gently on the bottom center of the mouse's back. Mice were video recorded for a duration of 5 min by a web or high-speed camera? The total number of scratching bouts, wipes and other behaviors in response to the tape were quantified.

Nape-pinch Assay

Mice were anesthetized using isoflurane, and the nape of the neck (~2 cm^2 area) was shaved using an electric trimmer. After 2-3 days, the mice were habituated for 15 minutes in a glass chamber of ~10 cm diameter. An alligator clip producing 340 g force was applied to the shaved nape skin fold. The animal was placed back into the chamber and video recorded using high-speed

camera (80-200 fps) for 60 s. The videos were analyzed to quantify the scratch bouts, headshakes, bilateral wipes, and attending duration/episodes.

Tail-immersion Assay

A mouse to be tested was restrained in a plastic 50 mL screw capped conical centrifuge tubes with several holes in the tube wall so that mouse can breathe normally. A 0.5 cm^2 opening was cut in the cap to allow the tail access to the water bath. Mice were habituated in the tube for 30 minutes in 2 days. On 3rd day, by holding the tube horizontal, the distal part of the tail (~4 cm) was submerged in the temperature-controlled water bath. Sudden tail-flick was used as a response sign. 3 trials were performed with an interval of 15 minutes. The tail-flick latencies of the three trials were recorded using a stopwatch and averaged for quantification. Cutoff time was 10 s. The test was performed at a gap of 24 h for 3 temperatures (48, 50 and 55 ℃).

Peripheral optogenetics, high-speed imaging, and pain score

To study several sub-second behavioral phenotypes of *Split*^{Cre}-A*β ReaChR* mice after peripheral light-stimulation of different body parts, we used a high-speed camera (FASTCAM UX100 800K-M-4GB - Monochrome 800K with 4GB memory) with an attached zoom lens (Nikon Zoom Wide Angle Tele-photo 24-85mm f2.8) on a tripod as previously described (Abdus-Saboor et al., 2019; Abdus-Saboor and Luo, 2022; Cui et al., 2022). Behaviors were recorded at 100-1000 frames per second (fps) with different resolutions as per the demand

of the behavior test. A far red-shifted LED light that mice cannot detect was used to help the video quality. Mice were acclimated on an elevated perforated wire-mesh platform daily for 1 h in transparent rectangular Plexiglas chambers either for 2 (Plantar stimulation) or 3 days (after shaving the nape of the neck and back). On the day of the experiment, they were habituated for 45 min before peripheral 473 nm blue laser (Shanghai Laser and Optics Century, BL473T8-150FC/ADR-800A) stimulation. When mouse was still, a blue laser (5-20 mW, 10 Hz square wave, waveform generator (hp Hewlett Packard 15MHZ Function Waveform Generator, 33210A)), was shined upon the plantar surface below the wire-mesh space (the distance between paw and the laser cord-outlet tip is ~2 mm). Laser intensity was measured using a Digital Optical Power Meter with a 9.5 mm aperture (ThorLabs, PM100A). Each mouse was tested for 5 trials with an inter-trial interval of 5 min. The percentage of trials showing paw withdrawal response, such as the paw flutter, flick, lick or the brisk withdrawal of the paw, was quantified. The paw-withdrawal latency (s) in response to the plantar optogenetic stimulation was also quantified and averaged from 5 trials.

For optical stimuli of the tail, when the mouse was not grooming and its tail was at complete rest, the mid of the tail was stimulated by shining a blue laser from ~2 mm distance below the wire-mesh. Each mouse was tested for 5 trials with an inter-trial interval of 5 min. The latency to flick the tail and the percentage of trails showing withdrawal response were quantified and averaged from 5 trials.

For optical stimuli of the nape and back, mice were shaved at these regions using an electric trimmer and then habituated for 3 days under transparent plexiglas chambers. Nape or back of these mice were stimulated from upside of the chamber by a blue laser when they were still. Any sudden body-movement/shaking or avoidance behaviors of the mice was considered as a positive response. Each mouse was tested for 5 trials with an inter-trial interval of 5 min. The latency to flick the tail and the percentage of trails showing withdrawal response were quantified and averaged from 5 trials.

The pain score was quantified as previously described (Abdus-Saboor et al., 2019). Briefly, four individual behavior features: orbital tightening, hind paw shake, hind paw guarding, and jumping were considered as “pain” related behaviors, and 1 score was given for each behavior shown (0 minimum and 4 maximum score) for a testing trial. The final pain score was averaged from all five trials.

Conditioned Place Preference Assay

A chamber with two compartments separated by a smaller central compartment was designed. The two big chambers’ walls had distinctive visual cue patterns (white and black stripes vs white checkered duct tapes). The apparatus was placed over the elevated wire-mesh platform. Each mouse was allowed 20 minutes to explore the three-chambered apparatus with no optogenetic stimulation for 3 days. The mouse was excluded from the study if it showed more than 60% preference to a particular chamber at this stage. From days 4-6,

whenever mouse entered a specific chamber (White strips pattern on the wall), a blue laser (5 mW, 10 Hz) was shined on the plantar surface of the treated hind paw (either saline- or CFA-treated) from below the wire mesh platform till the mouse leaves this chamber and reach to the other chamber. To avoid any prospective optic cable and hand movement-related non-specific response, the optic cable (held in the hand of the experimenter) was also moved under the platform with the movement of the mouse but the light was only shined when the mouse entered the stimulation chamber. This was repeated for 20 minutes from day 4-6. On day 7, we tested these mice for place preference where each mouse was allowed 20 minutes to freely move about the three-chambered apparatus without blue laser stimulation. The activity was recorded using a webcam from the upside and scored later using AnyMaze software. Percent post-stimulation change was calculated as percent time in blue light chamber after training minus percent time in blue light chamber before training.

Spinal light cannula implantation

A light cannula (Ceramic, 1.25 mm diameter, 200 µm optic core, and length ~ 0.25 mm, Thor Labs) was implanted in T11 region of the mouse spinal cord as described previously (Christensen et al., 2016). Briefly, under isoflurane anesthesia, the hairs of the back region of a mouse were removed, and the mouse was placed in a stereotax (Model 940, KOPF instruments, Tujunga, CA, USA). After sterilization of the surgical site, a local anesthetic was administered prior to the incision. For implantation at ~T11 region, a 1 cm long incision was

made starting caudal of the peak of the dorsal hump, extending approximately 0.5 cm rostral and 0.5 cm caudal from the initial incision site. White tendons were cut from both sides of spinal column and the vertebral column was exposed by clearing tissue from the transverse processes without damaging spinal cord and nerves. T11 vertebra was fixed from both sides using the spinal adapters (#51690, Stoelting Co., Wood Dale, IL). Surface connective tissue was removed from the T11 vertebra and the adjacent rostral and caudal vertebrae by gentle scrubbing using the tip of sterilized cotton swabs. With a fine tipped burr drill (0.5 mm in diameter), the bone and dura mater were punctured. A light cannula was prepared to implant. The hole surface was dried using the cotton swabs. Using the other side tip of the cotton applicator, a very little amount of glue (Krazy®Glue, Part #963257) was applied around burr-hole before lowering the cannula into place. After lowering the cannula through the hole, and once the cannula attaches to the spinal cord dorsal surface firmly, dental cement was applied around the outside of the vertebra to stabilize the cannula. Spinal fixation bars were removed after drying of the cement. The skin was sutured, followed by administration of systematic analgesics. Mouse was put on a warm pad for recovery. After surgery, each mouse was housed individually to avoid accidental removal of the light-cannula by a cage mate. Implanted mice were used for behavior assays 2 weeks after implantation.

Central/Spinal optogenetics

Two weeks after the spinal light-cannula implantation into *Split^{Cre}-Aβ ReaChR* mice, the light cannula was attached to a rotating fiber cannula connected to the blue laser. These mice were habituated on an elevated perforated wire-mesh platform daily for 1 h in a transparent circular Plexiglas chamber (7 cm diameter and 30 cm height) for 3 days. On 4th day, in the similar settings, after 45 min habituation, mice were stimulated by a blue laser of lower (0.5 mW) or higher intensity (10 mW) (an interval of 24 h between the two laser tests). The stimulation protocol ('n' mW, 10 Hz, square wave, 30 s on, 1 min off) was performed 10 times. VFH testing to check the mechanical sensitivity of the plantar surface was performed at 15 minutes before stimulation (baseline) and different time points (5, 30, 90 and 120 min) after stimulation. Mouse behaviors were recorded at 30 fps using a normal web camera (Logitech) to detect any spontaneous behavioral phenotype (Licking, scratching, etc.). Some mice were sacrificed for spinal c-Fos immunostaining in 90 minutes after the last stimulation. Control mice were sacrificed without light stimuli.

Mouse spinal cord vibratome sections and c-Fos immunostaining

The spinal cord tissues were vibratome sectioned for c-Fos immunostaining. In brief, after the transcardiac perfusion of mice in 4% PFA, their lower thoracic (T11) and lumbar (L4/5) spinal columns were collected and post fixed in 4% PFA for 1 h at 4 degree. After 3 X 5 min 1X PBS washes, the spinal segments were embedded in 2% low-melt agarose. Using a vibratome machine

(VT1200S, Leica Microsystems, Nussloch, Germany), 40 µm thickness spinal cord sections were cut. Sections were washed in PBS containing 0.5% TritonX-100 (3X 15 minutes), and then blocked in PBS containing 5% lamb serum and 0.5% TritonX-100 (PBT) for 1 hour at room temperature. Rabbit anti-c-Fos (1:800; Cell Signaling Technology) was diluted in the same buffer (1:800), and incubated for ~24 h at 4°C, then washed in PBT (3X 15 minutes). Secondary antibodies were incubated in blocking buffer at 1:500 dilution for 90 min at room temperature. Tissues were then washed in PBT (3x 15 minutes), followed by clearing in 50 and 75% glycerol in PBS (15 min each). Sections were mounted in 75% glycerol, and cover slip was sealed using clear nail-polish (Fisher Scientific, NC1849418).

Quantification, statistical analysis, software, and data presentation

Electrophysiological data were analyzed using Clampfit 10 (Molecular Devices, Sunnyvale, CA, USA). Data were collected from 17 male and 14 female animals and were aggregated for data analysis. To confirm that impulses evoked by LED light and mechanical indenter are generated from the same fiber, the amplitudes and shapes of the impulses evoked by both LED light and mechanical indenter at the same receptive field were compared, and the data were included only when mechanically evoked impulses matched the light-evoked impulses. Conduction velocity was calculated by the distance

between stimulation site and recording site divided by the time latency for eliciting an impulse following electrical stimulation.

All data shown in column and line graphs represent Mean ± SEM, unless otherwise mentioned. Sample sizes and statistical methods are defined in respective figure legends. Counting of cell-number was performed in FIJI software (NIH). All data were analyzed, and graphs were originally created using GraphPad Prism Version 9.4.1 and further modified for publication purpose in Adobe Illustrator Version 27. Some cartoons in the figures were made using BioRender.com.

References

Abdus-Saboor, I., Fried, N.T., Lay, M., Burdge, J., Swanson, K., Fischer, R., Jones, J., Dong, P., Cai, W., Guo, X.*, et al.* (2019). Development of a Mouse Pain Scale Using Sub-second Behavioral Mapping and Statistical Modeling. Cell Rep *28*, 1623-1634 e1624.

Abdus-Saboor, I., and Luo, W. (2022). Measuring Mouse Somatosensory Reflexive Behaviors with High-speed Videography, Statistical Modeling, and Machine Learning. Neuromethods *178*, 441-456.

Alshahrani, S., Fernandez-Conti, F., Araujo, A., and DiFulvio, M. (2012). Rapid determination of the thermal nociceptive threshold in diabetic rats. J Vis Exp, e3785.

Arcourt, A., Gorham, L., Dhandapani, R., Prato, V., Taberner, F.J., Wende, H., Gangadharan, V., Birchmeier, C., Heppenstall, P.A., and Lechner, S.G. (2017). Touch Receptor-Derived Sensory Information Alleviates Acute Pain Signaling and Fine-Tunes Nociceptive Reflex Coordination. Neuron *93*, 179-193.

Brown, P.B., Gladfelter, W.E., Culberson, J.C., Covalt-Dunning, D., Sonty, R.V., Pubols, L.M., and Millecchia, R.J. (1991). Somatotopic organization of single primary afferent axon projections to cat spinal cord dorsal horn. J Neurosci *11*, 298-309.

Campbell, J.N., Raja, S.N., Meyer, R.A., and Mackinnon, S.E. (1988). Myelinated afferents signal the hyperalgesia associated with nerve injury. Pain *32*, 89-94.

Caylor, J., Reddy, R., Yin, S., Cui, C., Huang, M., Huang, C., Ramesh, R., Baker, D.G., Simmons, A., Souza, D.*, et al.* (2019). Spinal cord stimulation in chronic pain: evidence and theory for mechanisms of action. Bioelectron Med *5*.

Celik, E.C., Erhan, B., Gunduz, B., and Lakse, E. (2013). The effect of low-frequency TENS in the treatment of neuropathic pain in patients with spinal cord injury. Spinal Cord *51*, 334-337.

Chamessian, A., Matsuda, M., Young, M., Wang, M., Zhang, Z.J., Liu, D., Tobin, B., Xu, Z.Z., Van de Ven, T., and Ji, R.R. (2019). Is Optogenetic Activation of Vglut1-Positive Abeta Low-Threshold Mechanoreceptors Sufficient to Induce Tactile Allodynia in Mice after Nerve Injury? J Neurosci *39*, 6202-6215.

Chaplan, S.R., Bach, F.W., Pogrel, J.W., Chung, J.M., and Yaksh, T.L. (1994). Quantitative assessment of tactile allodynia in the rat paw. J Neurosci Methods *53*, 55-63.

Choi, S., Hachisuka, J., Brett, M.A., Magee, A.R., Omori, Y., Iqbal, N.U., Zhang, D., DeLisle, M.M., Wolfson, R.L., Bai, L.*, et al.* (2020). Parallel ascending spinal pathways for affective touch and pain. Nature *587*, 258-263.

Christensen, A.J., Iyer, S.M., Francois, A., Vyas, S., Ramakrishnan, C., Vesuna, S., Deisseroth, K., Scherrer, G., and Delp, S.L. (2016). In Vivo Interrogation of Spinal Mechanosensory Circuits. Cell Rep *17*, 1699-1710.

Cohen, S.P., Vase, L., and Hooten, W.M. (2021). Chronic pain: an update on burden, best practices, and new advances. Lancet *397*, 2082-2097.

Crawford, L.K., and Caterina, M.J. (2020). Functional Anatomy of the Sensory Nervous System: Updates From the Neuroscience Bench. Toxicol Pathol *48*, 174-189.

Cui, L., Guo, J., Cranfill, S.L., Gautam, M., Bhattarai, J., Olson, W., Beattie, K., Challis, R.C., Wu, Q., Song, X.*, et al.* (2022). Glutamate in primary afferents is required for itch transmission. Neuron *110*, 809-823 e805.

Cui, L., Miao, X., Liang, L., Abdus-Saboor, I., Olson, W., Fleming, M.S., Ma, M., Tao, Y.X., and Luo, W. (2016). Identification of Early RET+ Deep Dorsal Spinal Cord Interneurons in Gating Pain. Neuron *91*, 1137-1153.

Devor, M. (2009). Ectopic discharge in Abeta afferents as a source of neuropathic pain. Exp Brain Res *196*, 115-128.

Dhandapani, R., Arokiaraj, C.M., Taberner, F.J., Pacifico, P., Raja, S., Nocchi, L., Portulano, C., Franciosa, F., Maffei, M., Hussain, A.F.*, et al.* (2018). Control of mechanical pain hypersensitivity in mice through ligand-targeted photoablation of TrkB-positive sensory neurons. Nat Commun *9*, 1640.

Duan-Mu, C.L., Zhang, X.N., Shi, H., Su, Y.S., Wan, H.Y., Wang, Y., Qu, Z.Y., He, W., Wang, X.Y., and Jing, X.H. (2021). Electroacupuncture-Induced Muscular Inflammatory Pain Relief Was Associated With Activation of Low-Threshold Mechanoreceptor Neurons and Inhibition of Wide Dynamic Range Neurons in Spinal Dorsal Horn. Front Neurosci *15*, 687173.

Duan, B., Cheng, L., Bourane, S., Britz, O., Padilla, C., Garcia-Campmany, L., Krashes, M., Knowlton, W., Velasquez, T., Ren, X.*, et al.* (2014). Identification of spinal circuits transmitting and gating mechanical pain. Cell *159*, 1417-1432.

Gardner, S.E., Blodgett, N.P., Hillis, S.L., Borhart, E., Malloy, L., Abbott, L., Pezzella, P., Jensen, M., Sommer, T., Sluka, K.A.*, et al.* (2014). HI-TENS reduces moderate-to-severe pain associated with most wound care procedures: a pilot study. Biol Res Nurs *16*, 310-319.

Gibson, W., Wand, B.M., Meads, C., Catley, M.J., and O'Connell, N.E. (2019). Transcutaneous electrical nerve stimulation (TENS) for chronic pain - an overview of Cochrane Reviews. Cochrane Database Syst Rev *4*, CD011890.

Gilbert, J.E., Zhang, T., Esteller, R., and Grill, W.M. (2022). Evaluating optimized temporal patterns of spinal cord stimulation (SCS). Brain Stimul *15*, 1051-1062.

Gray, J. A. B. and Matthews, P. B. C. (1951). A comparison of the adaptaion of the Pacinian corpuscle with the accommodation of its own axon. J. Physiol. (Lond.), 144, 454-464.

Hooks, B.M., Lin, J.Y., Guo, C., and Svoboda, K. (2015). Dual-channel circuit mapping reveals sensorimotor convergence in the primary motor cortex. J Neurosci *35*, 4418-4426.

Ishibashi, T., Yoshikawa, Y., Sueto, D., Tashima, R., Tozaki-Saitoh, H., Koga, K., Yamaura, K., and Tsuda, M. (2022). Selective Involvement of a Subset of Spinal Dorsal Horn Neurons Operated by a Prodynorphin Promoter in Abeta Fiber-Mediated Neuropathic Allodynia-Like Behavioral Responses in Rats. Front Mol Neurosci *15*, 911122.

Jensen, T.S., and Finnerup, N.B. (2014). A brief history of pain. Lancet Neurol *13*, 872.

Jin, D.M., Xu, Y., Geng, D.F., and Yan, T.B. (2010). Effect of transcutaneous electrical nerve stimulation on symptomatic diabetic peripheral neuropathy: a

meta-analysis of randomized controlled trials. Diabetes Res Clin Pract *89*, 10-15.

Karri, J., Joshi, M., Polson, G., Tang, T., Lee, M., Orhurhu, V., Deer, T., and Abd-Elsayed, A. (2020). Spinal Cord Stimulation for Chronic Pain Syndromes: A Review of Considerations in Practice Management. Pain Physician *23*, 599-616.

Koltzenburg, M., Lundberg, L.E.R., and Torebjork, E.H. (1992). Dynamic and static components of mechanical hyperalgesia in human hairy skin. Pain *51*, 207-219.

Li, L., Rutlin, M., Abraira, V.E., Cassidy, C., Kus, L., Gong, S., Jankowski, M.P., Luo, W., Heintz, N., Koerber, H.R.*, et al.* (2011). The functional organization of cutaneous low-threshold mechanosensory neurons. Cell *147*, 1615-1627.

Lin J.Y., Knutsen P.M., Muller A., Kleinfeld D., Tsien R.Y. (2013). ReaChR: a red-shifted variant of channelrhodopsin enables deep transcranial optogenetic excitation Nat. Neurosci. 16, 1499-1508.

Liu, C.N., Michaelis, M., Amir, R., and Devor, M. (2000). Spinal nerve injury enhances subthreshold membrane potential oscillations in DRG neurons: relation to neuropathic pain. J Neurophysiol *84*, 205-215.

Liu, Y., Latremoliere, A., Li, X., Zhang, Z., Chen, M., Wang, X., Fang, C., Zhu, J., Alexandre, C., Gao, Z.*, et al.* (2018). Touch and tactile neuropathic pain sensitivity are set by corticospinal projections. Nature *561*, 547-550.

Mancini, F., Bauleo, A., Cole, J., Lui, F., Porro, C.A., Haggard, P., and Iannetti, G.D. (2014). Whole-body mapping of spatial acuity for pain and touch. Ann Neurol *75*, 917-924.

Melzack, R., and Wall, P.D. (1965). Pain mechanisms: a new theory. Science *150*, 971-979.

Na, H.S., Leem, J.W., and Chung, J.M. (1993). Abnormalities of mechanoreceptors in a rat model of neuropathic pain: possible involvement in mediating mechanical allodynia. J Neurophysiol *70*, 522-528.

Niu, J., Ding, L., Li, J.J., Kim, H., Liu, J., Li, H., Moberly, A., Badea, T.C., Duncan, I.D., Son, Y.J.*, et al.* (2013). Modality-based organization of ascending somatosensory axons in the direct dorsal column pathway. J Neurosci *33*, 17691-17709.

Olson, W., Abdus-Saboor, I., Cui, L., Burdge, J., Raabe, T., Ma, M., Luo, W. (2017). Sparse genetic tracing reveals regionally specific functional organization of mammalian nociceptors. eLife 6, p. e29507

Price, T.J., and Gold, M.S. (2018). From Mechanism to Cure: Renewing the Goal to Eliminate the Disease of Pain. Pain Med *19*, 1525-1549.

Ranade, S.S., Woo, S.H., Dubin, A.E., Moshourab, R.A., Wetzel, C., Petrus, M., Mathur, J., Begay, V., Coste, B., Mainquist, J.*, et al.* (2014). Piezo2 is the major transducer of mechanical forces for touch sensation in mice. Nature *516*, 121-125.

Rutlin, M., Ho, C.Y., Abraira, V.E., Cassidy, C., Bai, L., Woodbury, C.J., and Ginty, D.D. (2014). The cellular and molecular basis of direction selectivity of Adelta-LTMRs. Cell *159*, 1640-1651.

Sant'Anna, M.B., Kusuda, R., Bozzo, T.A., Bassi, G.S., Alves-Filho, J.C., Cunha, F.Q., Ferreira, S.H., Souza, G.R., and Cunha, T.M. (2016). Medial plantar nerve ligation as a novel model of neuropathic pain in mice: pharmacological and molecular characterization. Sci Rep *6*, 26955.

Scott, S.A. (1992). Sensory neurons : diversity, development, and plasticity (New York: Oxford University Press).

Shealy, C.N., Mortimer, J.T., and Reswick, J.B. (1967). Electrical inhibition of pain by stimulation of the dorsal columns: preliminary clinical report. Anesth Analg *46*, 489-491.

Sonekatsu, M., Yamada, H., and Gu, J.G. (2020). Pressure-clamped single-fiber recording technique: A new recording method for studying sensory receptors. Mol Pain *16*, 1744806920927852.

Sun, H., Ren, K., Zhong, C.M., Ossipov, M.H., Malan, T.P., Lai, J., and Porreca, F. (2001). Nerve injury-induced tactile allodynia is mediated via ascending spinal dorsal column projections. Pain *90*, 105-111.

Sun, W., Jin, Y., Liu, H., Yang, D., Sun, T., Wang, Y., Fan, Y., Fan, X., Jin, X., Wan, L.*, et al.* (2022). Short-term spinal cord stimulation is an effective therapeutic approach for herpetic-related neuralgia-A Chinese nationwide expert consensus. Front Aging Neurosci *14*, 939432.

Tashima, R., Koga, K., Sekine, M., Kanehisa, K., Kohro, Y., Tominaga, K., Matsushita, K., Tozaki-Saitoh, H., Fukazawa, Y., Inoue, K.*, et al.* (2018). Optogenetic Activation of Non-Nociceptive Abeta Fibers Induces Neuropathic Pain-Like Sensory and Emotional Behaviors after Nerve Injury in Rats. eNeuro *5*.

Tonomura, S., Ling, J., and Gu, J.G. (2022). Function of KCNQ2 channels at nodes of Ranvier of lumbar spinal ventral nerves of rats. Mol Brain *15*, 64.

Vance, C.G., Rakel, B.A., Blodgett, N.P., DeSantana, J.M., Amendola, A., Zimmerman, M.B., Walsh, D.M., and Sluka, K.A. (2012). Effects of transcutaneous electrical nerve stimulation on pain, pain sensitivity, and function in people with knee osteoarthritis: a randomized controlled trial. Phys Ther *92*, 898-910.

Xu, Z.Z., Kim, Y.H., Bang, S., Zhang, Y., Berta, T., Wang, F., Oh, S.B., and Ji, R.R. (2015). Inhibition of mechanical allodynia in neuropathic pain by TLR5-mediated A-fiber blockade. Nat Med *21*, 1326-1331.

Figure 1

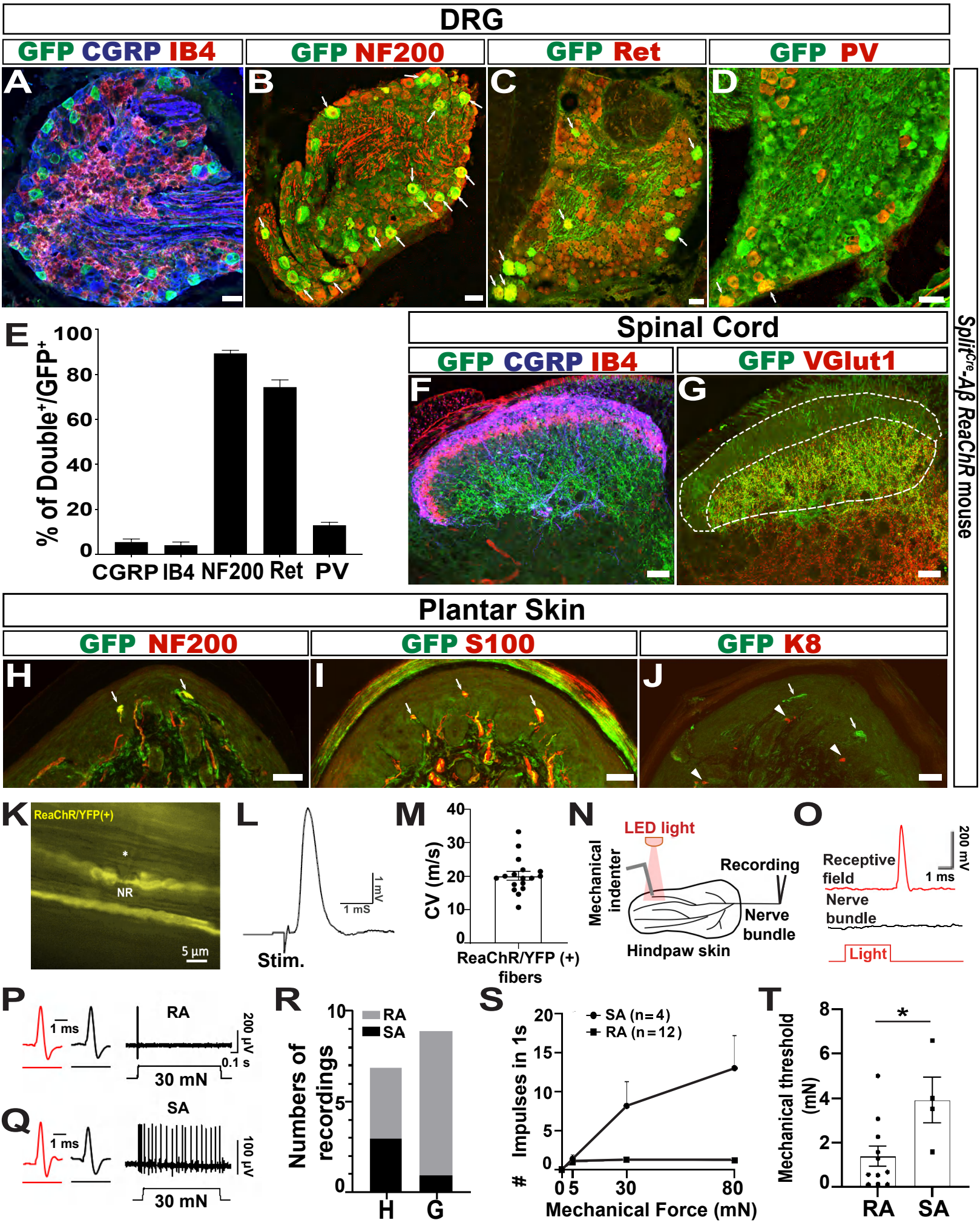
DRG
GFP CGRP IB4
GFP NF200
GFP Ret
GFP PV
A
B
C
D
E
% of Double+/GFP+
100
80
60
40
20
0
CGRP IB4 NF200 Ret PV
Spinal Cord
GFP CGRP IB4
GFP VGlut1
F
G
Plantar Skin
GFP NF200
GFP S100
GFP K8
H
I
J
Split^Cre-Aβ ReaChR mouse
K
ReaChR/YFP(+)
NR
5 µm
L
1 mV
1 mS
Stim.
M
CV (m/s)
40
30
20
10
0
ReaChR/YFP (+) fibers
N
LED light
Mechanical indenter
Recording
Nerve bundle
Hindpaw skin
O
200 mV
Receptive field
1 ms
Nerve bundle
Light
P
1 ms
RA
200 µV
0.1 s
30 mN
Q
1 ms
SA
100 µV
30 mN
R
Numbers of recordings
10
5
0
RA
SA
H
G
S
Impulses in 1s
20
15
10
5
0
SA (n=4)
RA (n=12)
0 5 30 80
Mechanical Force (mN)
T
Mechanical threshold (mN)
8
6
4
2
0
*
RA
SA

Figure 2

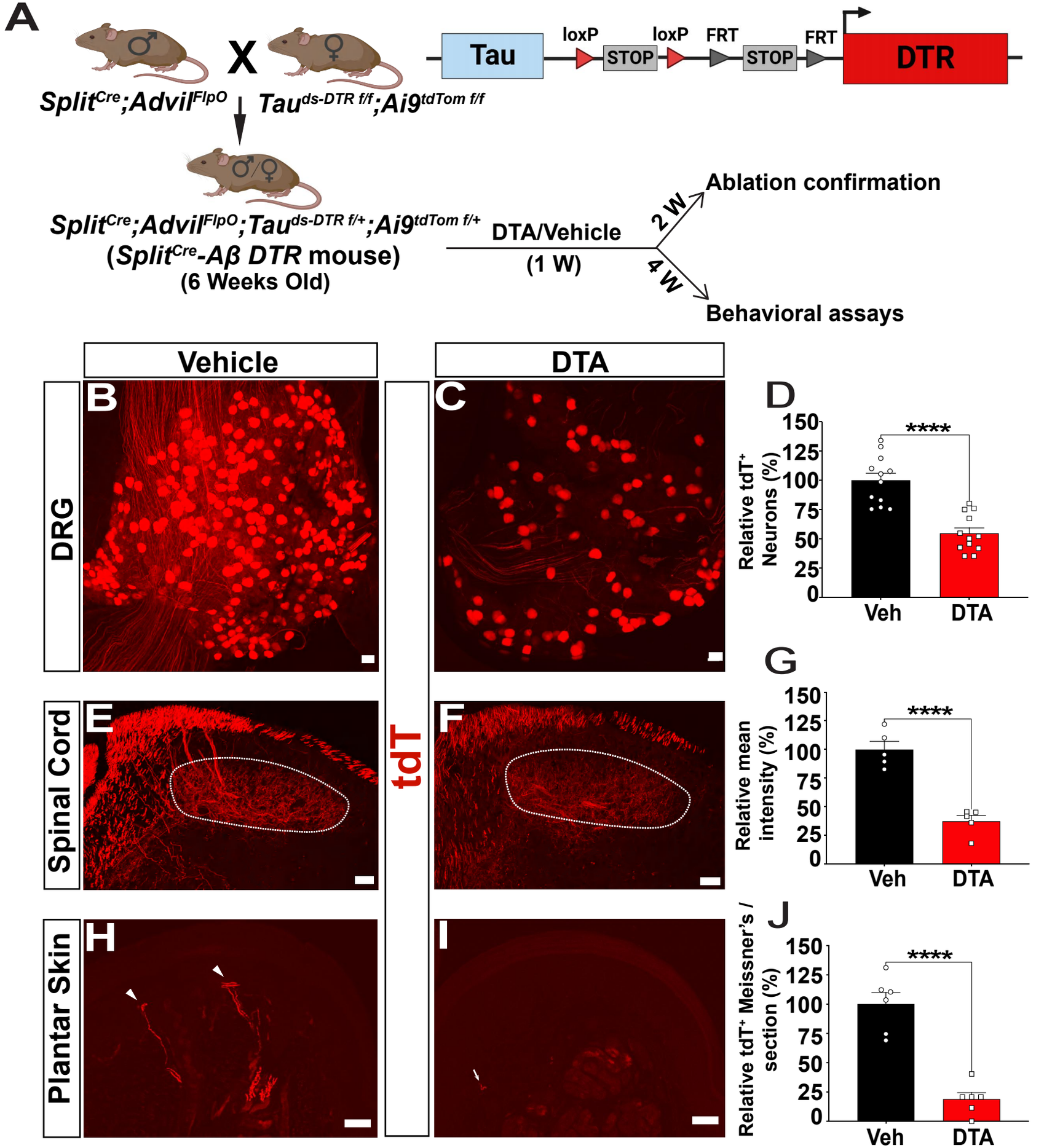
A
Split^Cre;Advil^FlpO
X
Tau^ds-DTR f/f;Ai9^tdTom f/f
Split^Cre;Advil^FlpO;Tau^ds-DTR f/+;Ai9^tdTom f/+
(Split^Cre-Aβ DTR mouse)
(6 Weeks Old)
Tau
loxP
STOP
loxP
FRT
STOP
FRT
DTR
DTA/Vehicle
(1 W)
2 W
4 W
Ablation confirmation
Behavioral assays
Vehicle
DTA
DRG
Spinal Cord
Plantar Skin
tdT
B
C
D
E
F
G
H
I
J
Relative tdT+ Neurons (%)
Relative mean intensity (%)
Relative tdT+ Meissner's / section (%)
150
125
100
75
50
25
0
****
Veh
DTA

Figure 3

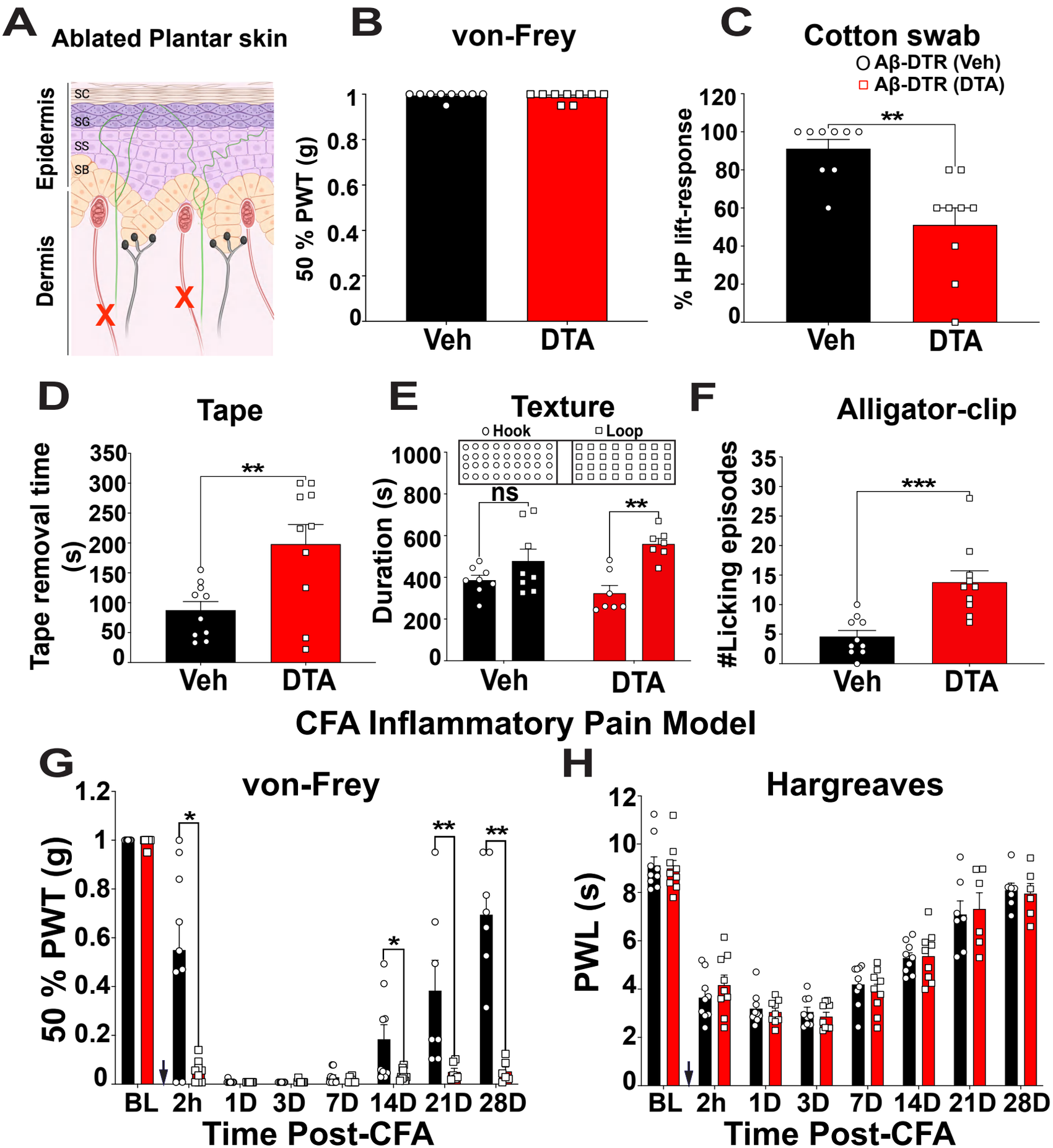
A
Ablated Plantar skin
Epidermis
Dermis
SC
SG
SS
SB
B
von-Frey
50 % PWT (g)
Veh
DTA
C
Cotton swab
Aβ-DTR (Veh)
Aβ-DTR (DTA)
% HP lift-response
**
Veh
DTA
D
Tape
Tape removal time (s)
**
Veh
DTA
E
Texture
Hook
Loop
Duration (s)
ns
**
Veh
DTA
F
Alligator-clip
#Licking episodes
***
Veh
DTA
CFA Inflammatory Pain Model
G
von-Frey
50 % PWT (g)
BL
2h
1D
3D
7D
14D
21D
28D
Time Post-CFA
H
Hargreaves
PWL (s)
BL
2h
1D
3D
7D
14D
21D
28D
Time Post-CFA

Figure 4

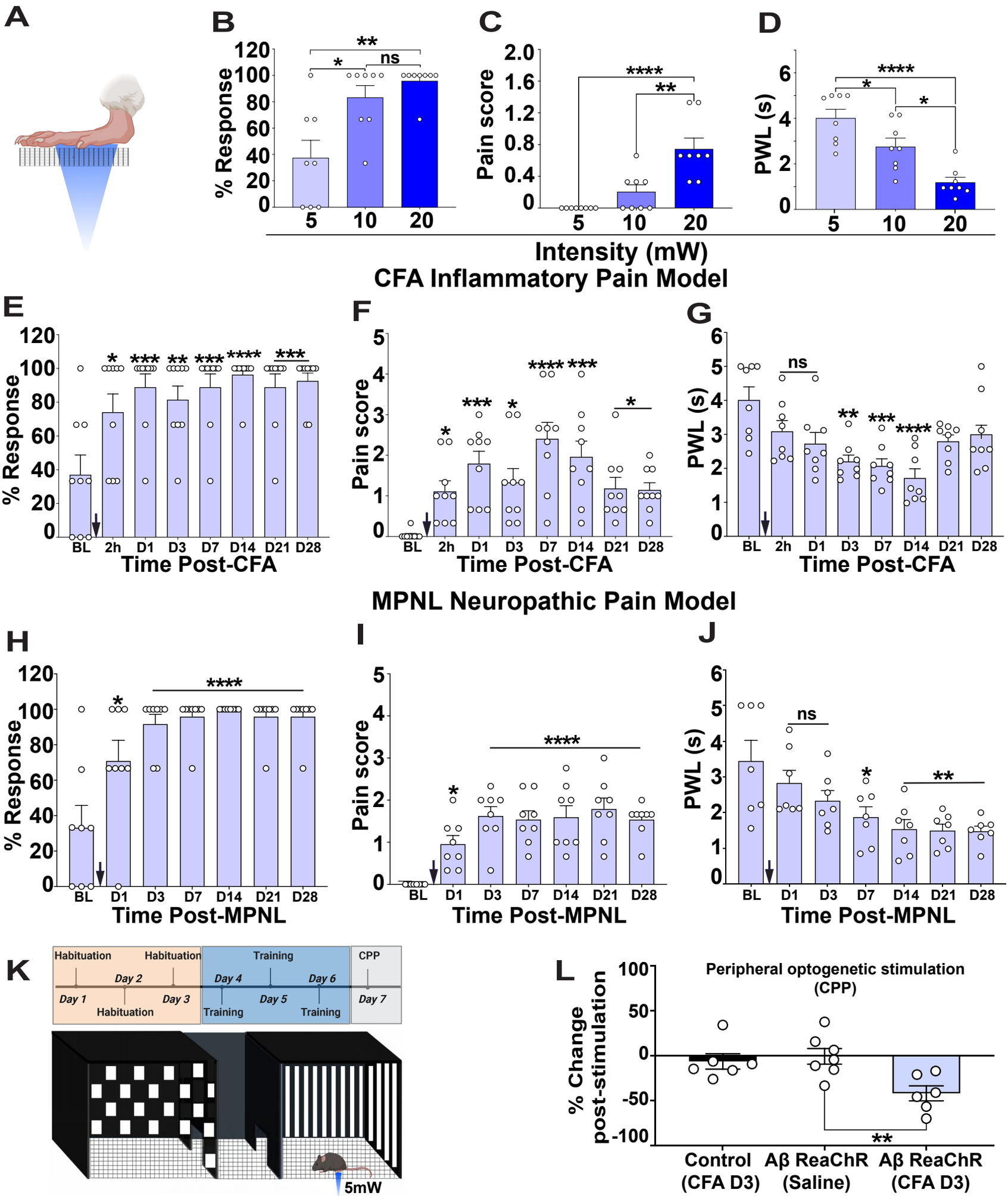
A
B
% Response
120
100
80
60
40
20
0
**
*
ns
5
10
20
C
Pain score
2.0
1.6
1.2
0.8
0.4
0
****
**
D
PWL (s)
6
4
2
0
****
*
*
Intensity (mW)
CFA Inflammatory Pain Model
E
% Response
*
***
**
***
****
***
BL
2h
D1
D3
D7
D14
D21
D28
Time Post-CFA
F
Pain score
*
***
*
****
***
*
Time Post-CFA
G
PWL (s)
ns
**
***
****
Time Post-CFA
MPNL Neuropathic Pain Model
H
% Response
*
****
Time Post-MPNL
I
Pain score
*
****
Time Post-MPNL
J
PWL (s)
ns
*
**
Time Post-MPNL
K
Habituation
Habituation
Training
CPP
Day 1
Day 2
Day 3
Day 4
Day 5
Day 6
Day 7
Habituation
Training
Training
5mW
L
Peripheral optogenetic stimulation
(CPP)
% Change
post-stimulation
100
50
0
-50
-100
**
Control
(CFA D3)
Aβ ReaChR
(Saline)
Aβ ReaChR
(CFA D3)

Figure 5

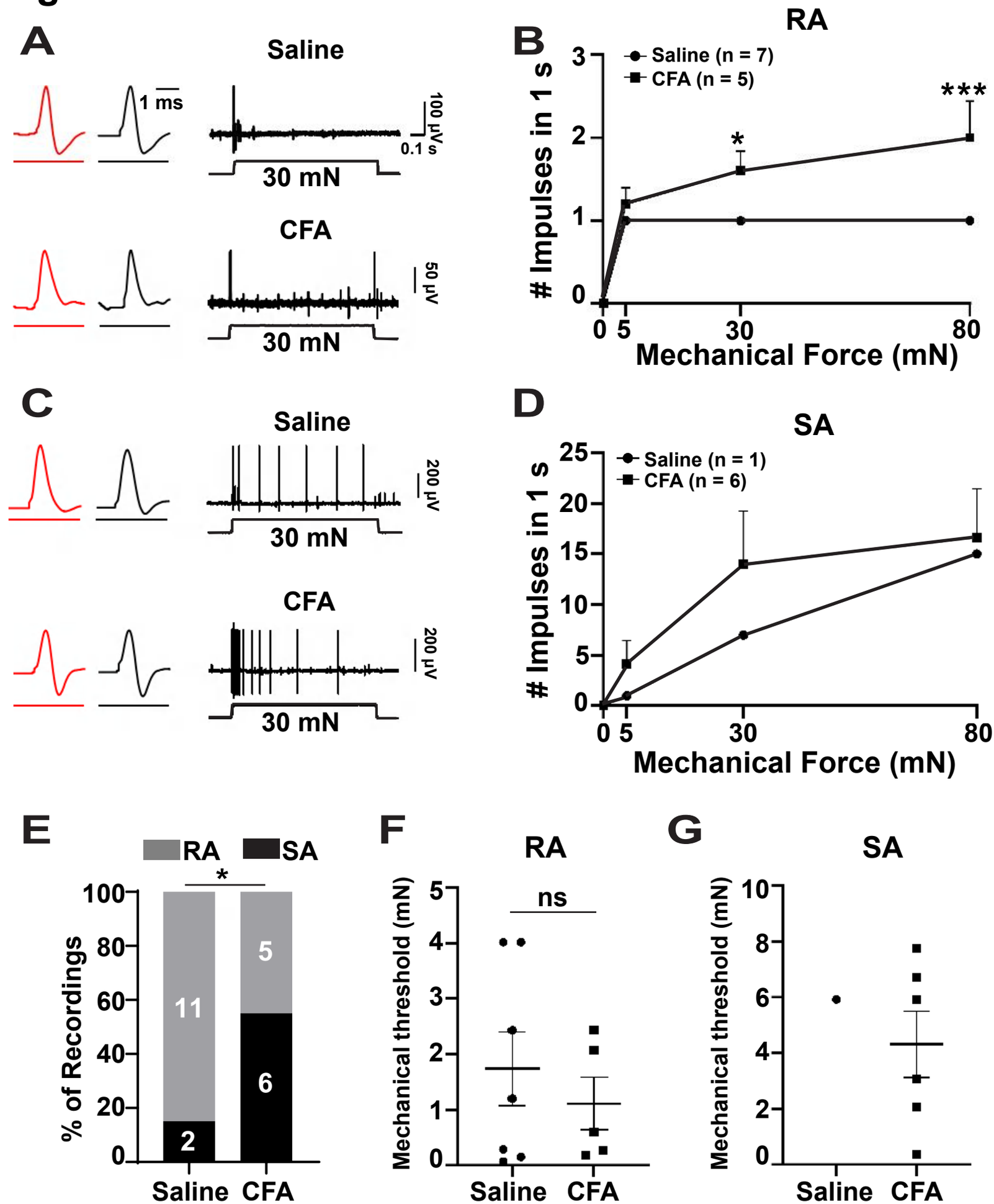
A
Saline
1 ms
100 µV
0.1 s
30 mN
CFA
50 µV
30 mN
B
RA
Saline (n = 7)
CFA (n = 5)
Impulses in 1 s
Mechanical Force (mN)
0 5 30 80
*
***
C
Saline
200 µV
30 mN
CFA
200 µV
30 mN
D
SA
Saline (n = 1)
CFA (n = 6)
Impulses in 1 s
Mechanical Force (mN)
0 5 30 80
E
RA
SA
*
% of Recordings
11
2
5
6
Saline CFA
F
RA
ns
Mechanical threshold (mN)
Saline CFA
G
SA
Mechanical threshold (mN)
Saline CFA

Figure 6

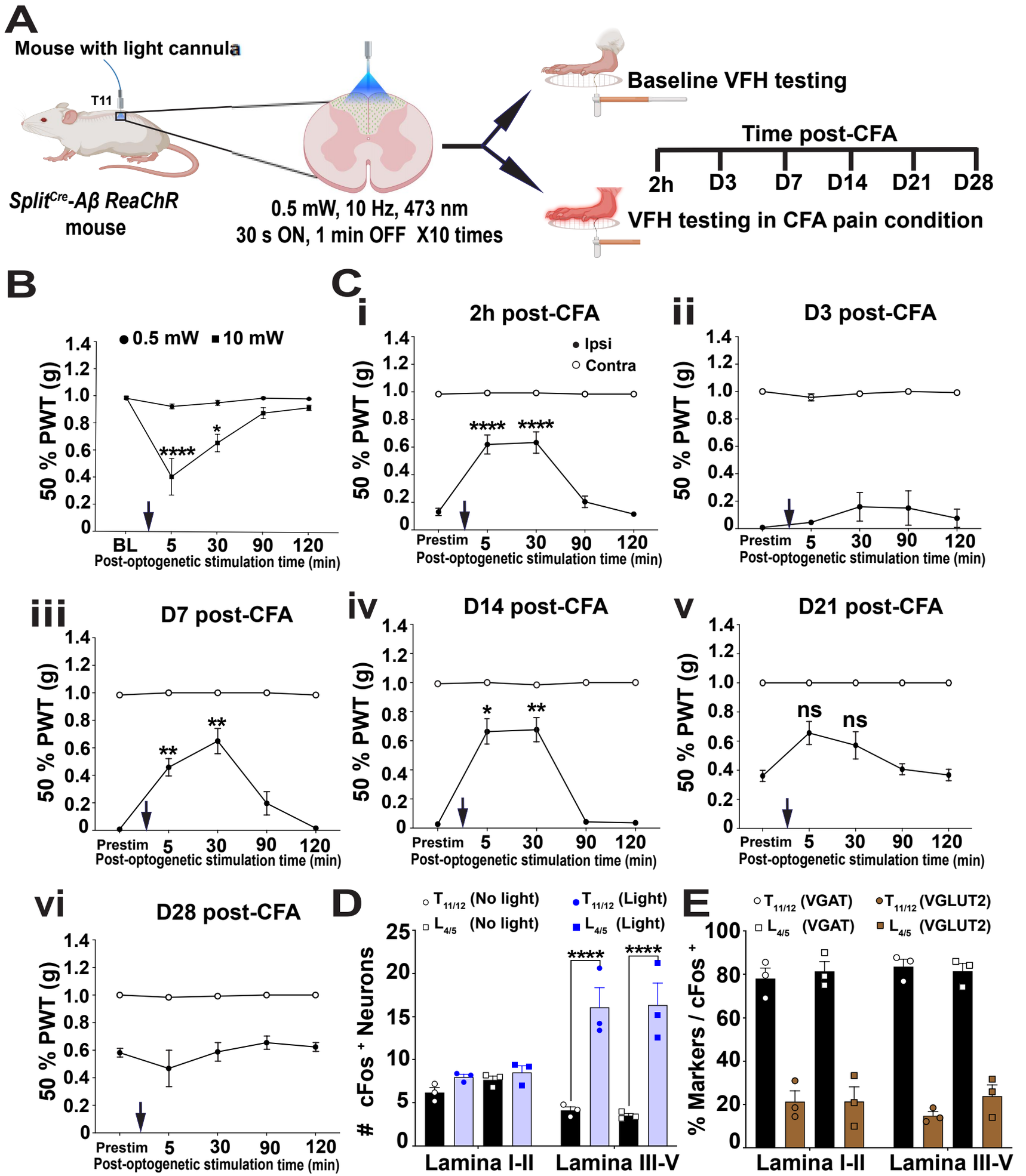
A
Mouse with light cannula
T11
Split^Cre-Aβ ReaChR mouse
0.5 mW, 10 Hz, 473 nm
30 s ON, 1 min OFF X10 times
Baseline VFH testing
Time post-CFA
2h
D3
D7
D14
D21
D28
VFH testing in CFA pain condition
B
0.5 mW
10 mW
50 % PWT (g)
BL
5
30
90
120
Post-optogenetic stimulation time (min)
C
i
2h post-CFA
Ipsi
Contra
ii
D3 post-CFA
iii
D7 post-CFA
iv
D14 post-CFA
v
D21 post-CFA
Prestim
ns
vi
D28 post-CFA
D
T11/12 (No light)
L4/5 (No light)
T11/12 (Light)
L4/5 (Light)
cFos+ Neurons
Lamina I-II
Lamina III-V
E
T11/12 (VGAT)
L4/5 (VGAT)
T11/12 (VGLUT2)
L4/5 (VGLUT2)
% Markers / cFos+

Figure 7

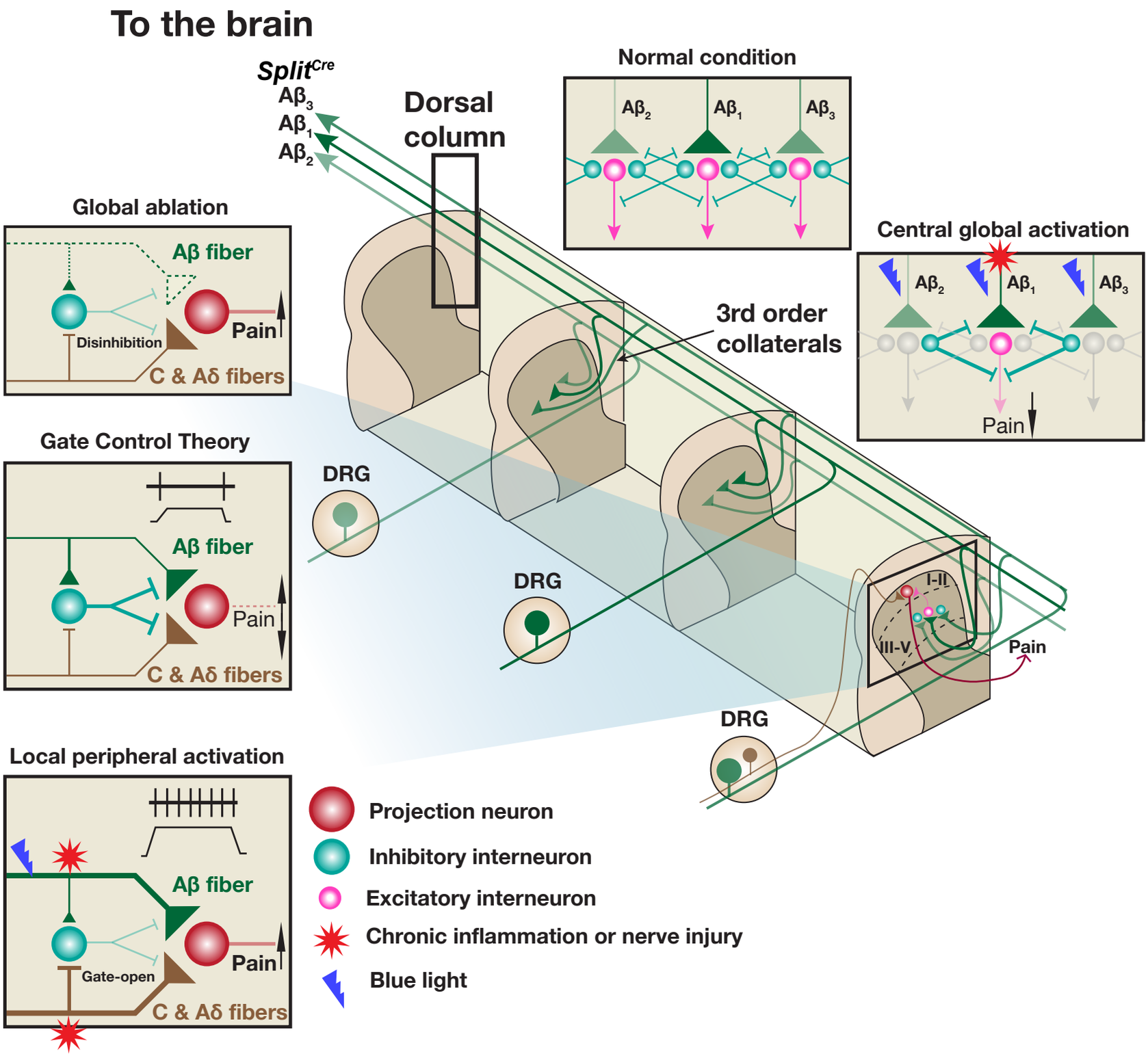
To the brain
Split^Cre
Aβ3
Aβ1
Aβ2
Dorsal column
Normal condition
Aβ2
Aβ1
Aβ3
Global ablation
Aβ fiber
Disinhibition
Pain
C & Aδ fibers
Central global activation
Aβ2
Aβ1
Aβ3
Pain
3rd order collaterals
Gate Control Theory
Aβ fiber
Pain
C & Aδ fibers
DRG
DRG
DRG
I-II
III-V
Pain
Local peripheral activation
Aβ fiber
Gate-open
Pain
C & Aδ fibers
Projection neuron
Inhibitory interneuron
Excitatory interneuron
Chronic inflammation or nerve injury
Blue light

Supplemental Information – Table of Contents

1. Supplemental Tables

Table S1, related to Figure 3: Summary of different thermal assays with control and ablated *Split^{Cre}-Aβ TauDTR* mice.

Table S2, related to Figure 4: Summary of peripheral light-evoked behavioral responses of *Split^{Cre}-Aβ ReaChR* mice.

Table S3, related to Figure 6: Summary of spinal light-evoked spontaneous behavioral responses of *Split^{Cre}-Aβ ReaChR* mice.

2. Supplemental Figures

Figure S1, related to Figure 1: Histological characterizations of *Split^{Cre}-Aβ ReaChR* mice.

Figure S2, related to Figure 2: Histological characterization of *Split^{Cre}-Aβ TauDTR* mice.

Figure S3, related to Figure 3: Ablation of Split^{Cre}-Aβ-LTMRs did not alter general locomotion and thermal sensation.

Figure S4, related to Figure 3: Ablation of Split^{Cre}-Aβ-LTMRs altered the gentle touch and nociception in the hairy skin.

Figure S5, related to Figure 4: Local optogenetic activation of Split^{Cre}-Aβ-LTMRs at different skin areas, and CFA-induced inflammation altered the GFP^{+} fiber innervation in plantar skin.

Figure S6, related to Figure 6: Dorsal column activation of Split^{Cre}-ReaChR^{+} Aβ-LTMRs evoked spinal cord dorsal horn neurons.

1. Supplemental Tables

Table S1. Summary of different thermal assays in *Split^{Cre}-Aβ TauDTR* mice, related to Figure 3.

Hargreaves			
Vehicle	9.89 ± 0.47 s		
DTA	10.29 ± 0.75 s		
Dry-ice			
Vehicle	2.77 ± 0.05 s		
DTA	2.65 ± 0.08 s		
Dynamic hotplate			
Vehicle	49.4 ± 0.24℃		
DTA	49.73 ± 0.30℃		
Static hotplate			
	Flick	**Lick**	**Jump**
Vehicle	10.33 ± 0.81 s	22.01 ± 2.23 s	29.33 ± 0.58 s
DTA	9.79 ± 0.77 s	21.34 ± 2.47 s	29.83 ± 0.17 s
Tail-immersion			
	48℃	**50℃**	**55℃**
Vehicle	1.91 ± 0.07 s	1.26 ± 0.03 s	0.71 ± 0.02 s
DTA	1.83 ± 0.05 s	1.33 ± 0.04 s	0.72 ± 0.02 s

Table S2. Summary of peripheral light-evoked behavioral response in *Split^{Cre}*-Aβ *ReaChR* mice, related to Figure 4.

Baseline						
	5 mW		10 mW		20 mW	
	Response (%)	Latency (s)	Response (%)	Latency (s)	Response (%)	Latency (s)
Hind paw	37.5 ± 13.27	4.01 ± 0.38	83.33 ± 8.9	2.76 ± 0.38	95.83 ± 4.17	1.88 ± 0.22
Tail	83.33 ± 8.9	2.82 ± 0.42	91.67 ± 5.45	1.78 ± 0.24	95.83 ± 4.17	0.78 ± 0.16

CFA-induced chronic inflammatory pain condition			
5 mW			
Time post-CFA	**Paw withdrawal frequency (%)**	**Latency (s)**	**Pain-score**
Baseline	37.03 ± 11.71	4.01 ± 0.38	0.04 ± 0.04
2h	74.07 ± 10.80	3.09 ± 0.31	1.11 ± 0.26
D1	88.89 ± 7.86	2.73 ± 0.33	1.79 ± 0.30
D3	81.48 ± 8.07	2.20 ± 0.19	1.33 ± 0.34
D7	88.89 ± 7.86	2.07 ± 0.21	2.41 ± 0.40
D14	96.30 ± 3.70	1.72 ± 0.27	1.96 ± 0.39
D21	88.89 ± 7.86	2.80 ± 0.19	1.18 ± 0.27
D28	92.59 ± 4.90	3.00 ± 0.39	1.15 ± 0.18

MPNL-induced chronic neuropathic pain condition			
5 mW			
Time post-MPNL	**Paw withdrawal frequency (%)**	**Latency (s)**	**Pain-score**
Baseline	33.17 ± 12.57	3.44 ± 0.58	0
D1	70.83 ± 11.68	2.83 ± 0.35	0.95 ± 0.20
D3	91.67 ± 5.46	2.33 ± 0.29	1.62 ± 0.22
D7	95.83 ± 4.17	1.87 ± 0.29	1.54 ± 0.21
D14	100 ± 0	1.54 ± 0.27	1.59 ± 0.27
D21	95.83 ± 4.17	1.50 ± 0.18	1.79 ± 0.26
D28	95.83 ± 4.17	1.48 ± 0.14	1.54 ± 0.14

Table S3. Summary of spinal light-evoked behavioral responses in *Split^{Cre}*-Aβ *ReaChR* mice, related to Figure 6.

50% Paw withdrawal threshold (g)					
Intensity (mW)	**Pre-stim.**	**5 min.**	**30 min.**	**90 min.**	**120 min.**
0.5	0.985 ± 0.007	0.924 ± 0.017	0.953 ± 0.018	0.989 ± 0.007	0.986 ± 0.004
10	0.98 ± 0.009	0.405 ± 0.13	0.657 ± 0.064	0.88 ± 0.04	0.92 ± 0.02

	Behaviors during light stimuli (15-minute period)					
Intensity (mW)	**Back attending episodes**		**Hind paw licking episodes**		**Back scratching bouts**	
	Pre-stim.	**Stim.**	**Pre-stim.**	**Stim.**	**Pre-stim.**	**Stim.**
0.5	12.01 ± 4.35	38.0 ± 9.05	1.14 ± 0.40	1.87 ± 0.55	7.14 ± 1.72	12.71 ± 3.67

2. Supplemental Figures

Figure S1. Related to Figure 1

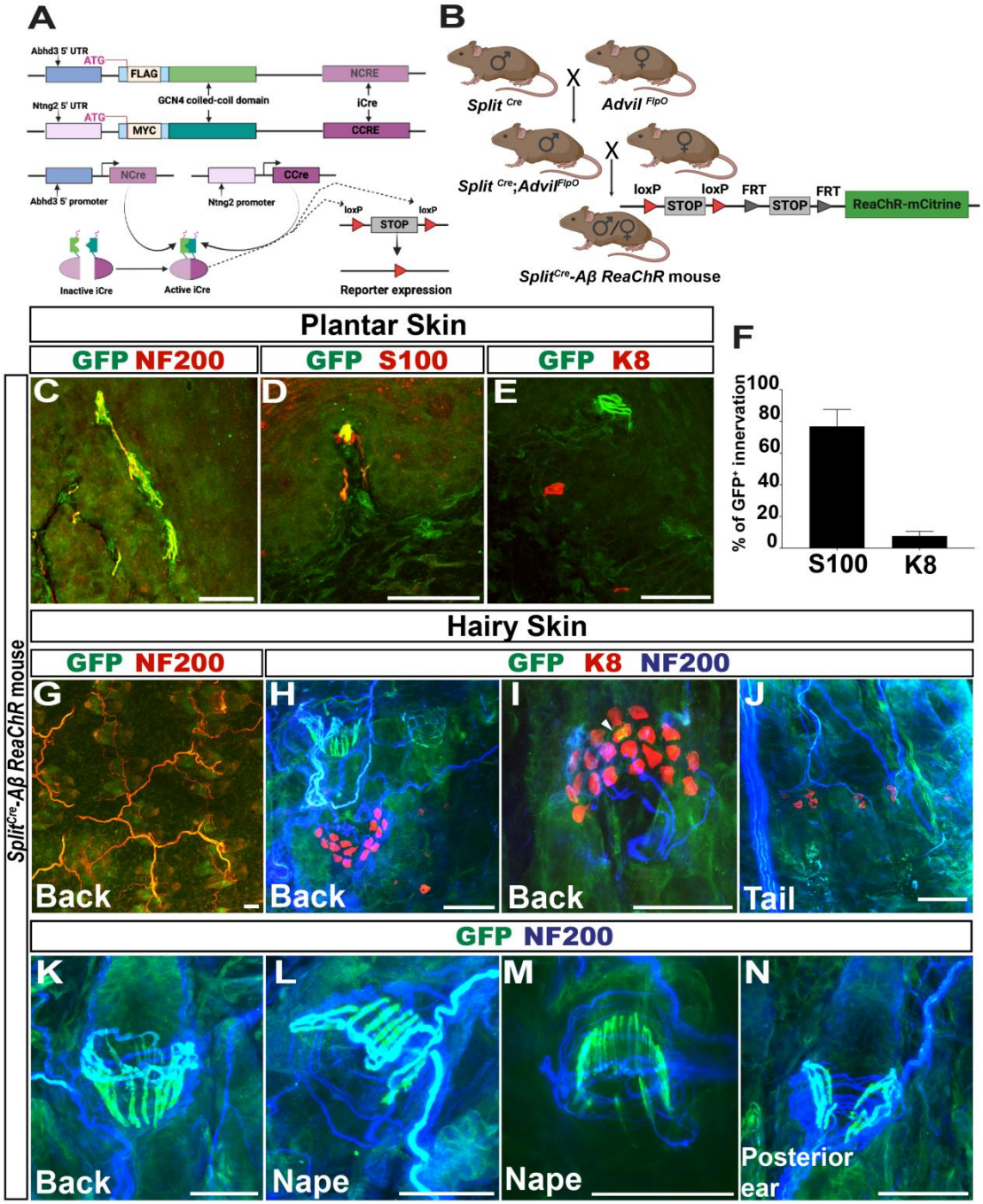

Figure S2. Related to Figure 2

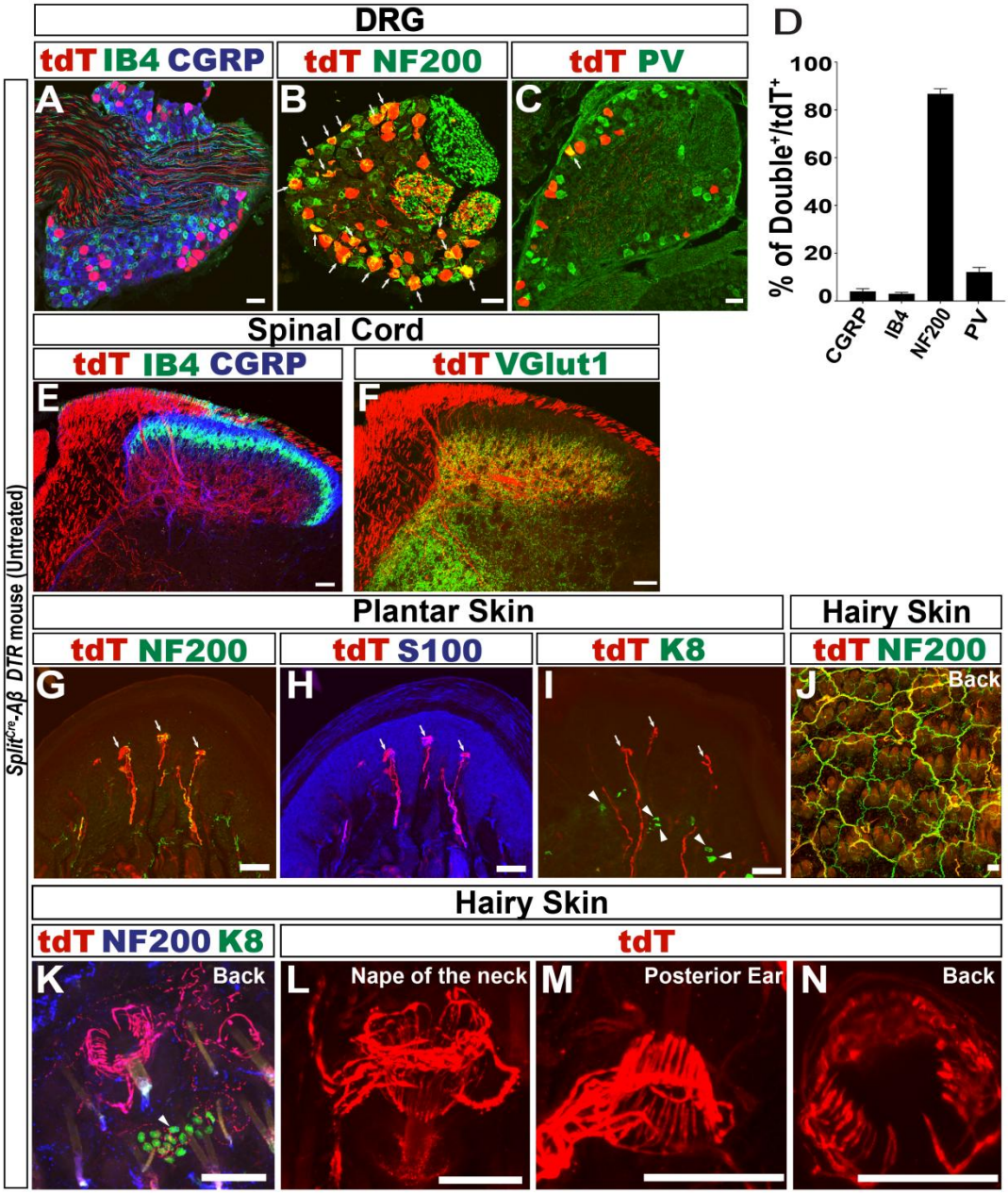

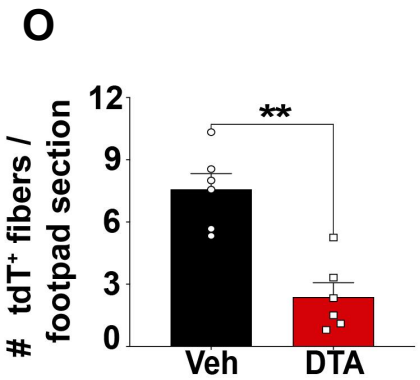

Figure S3. Related to Figure 3

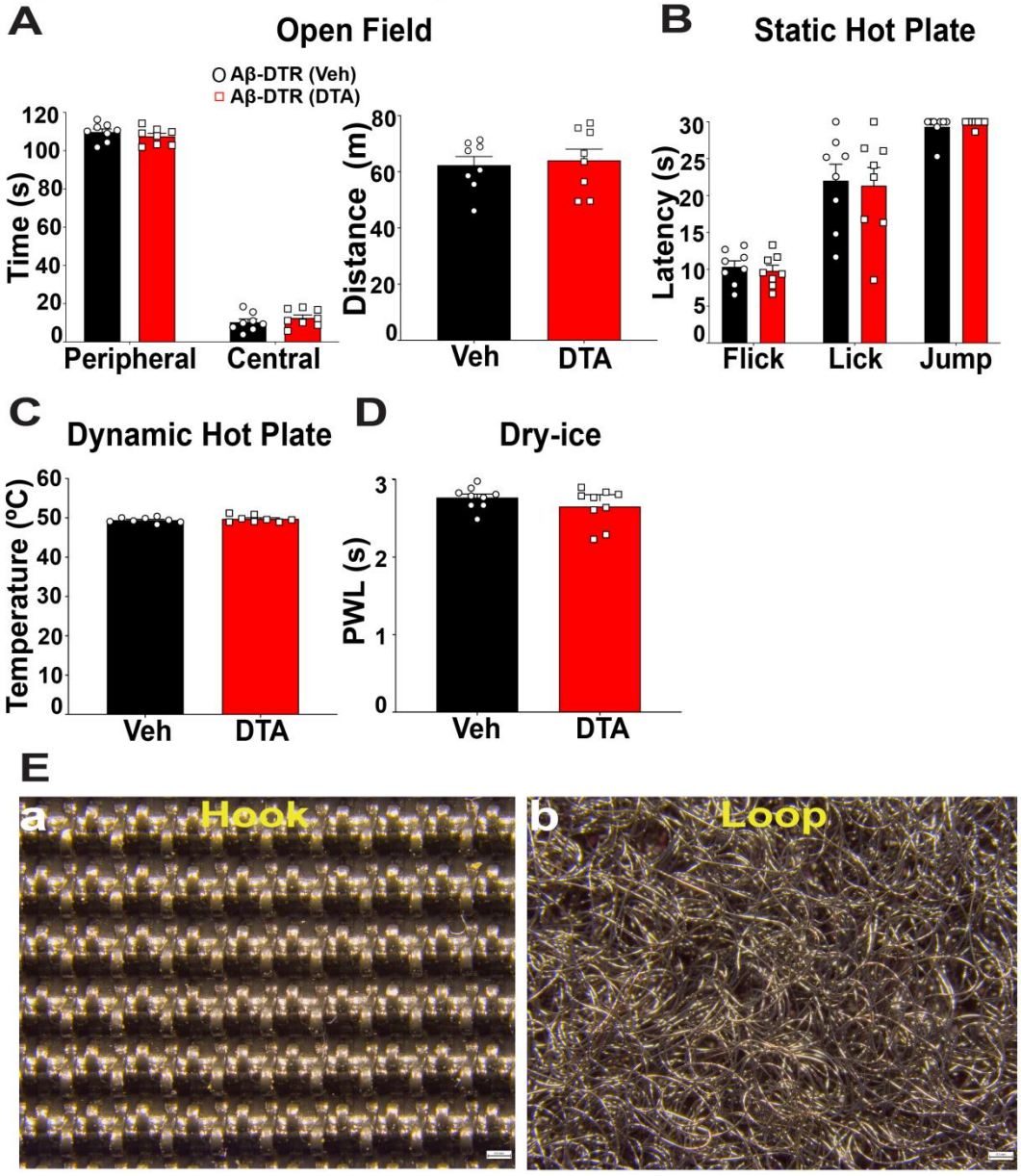

Figure S4. Related to Figure 3

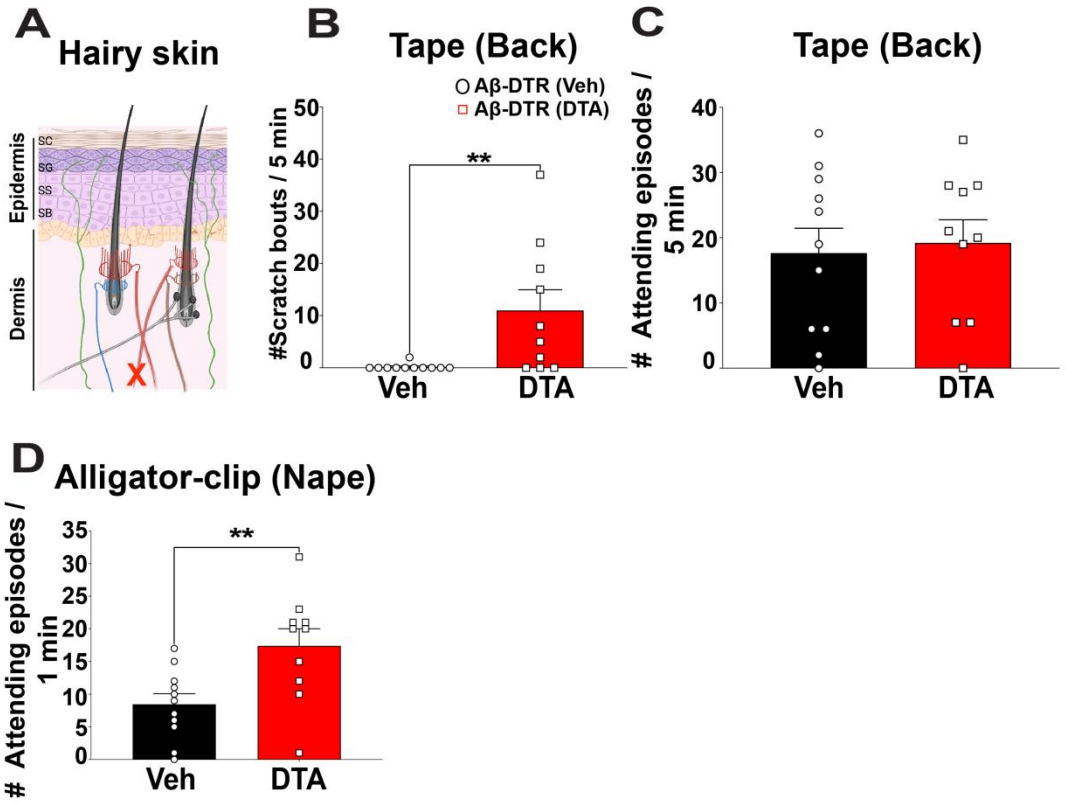

Figure S5. Related to Figure 4

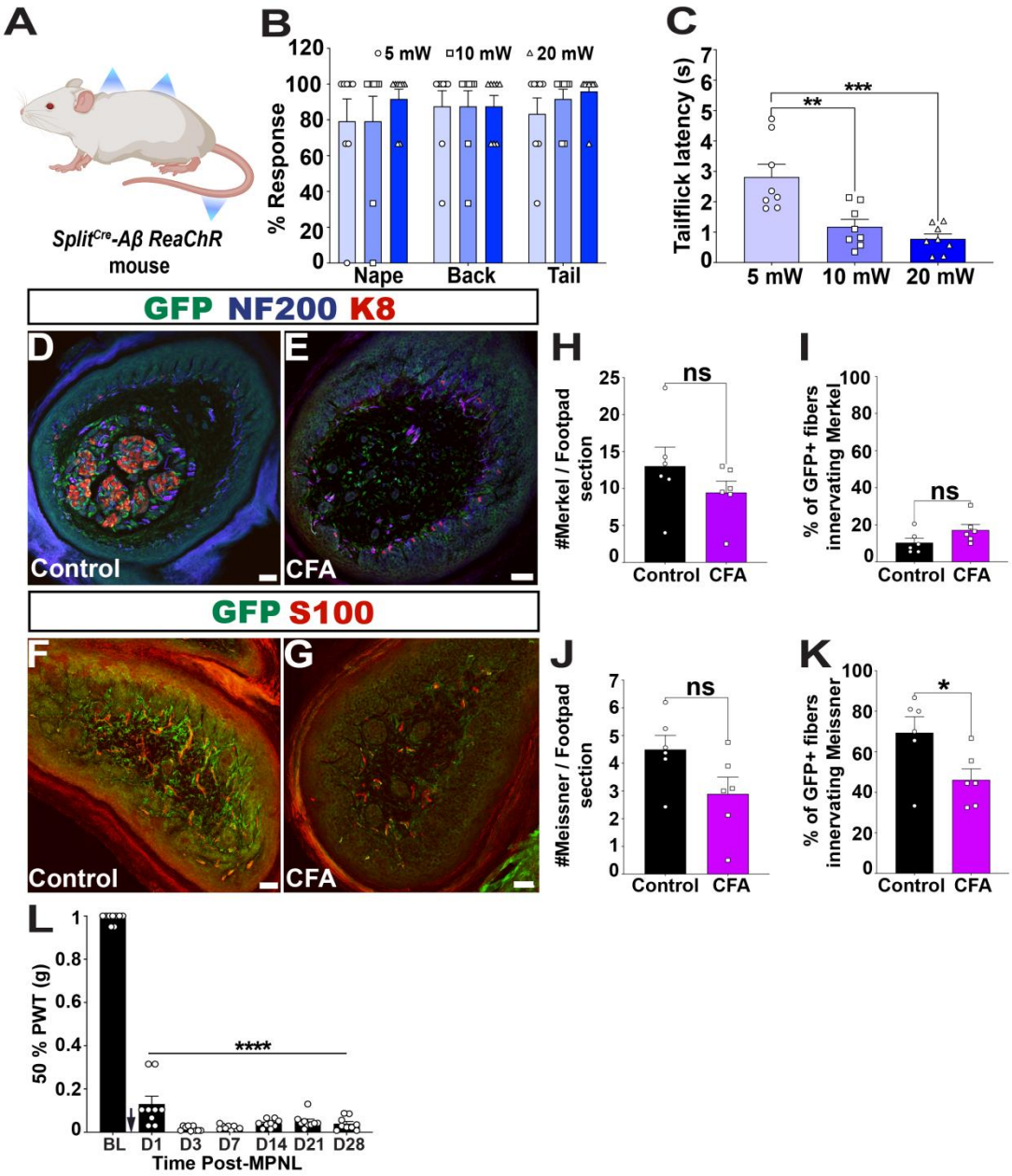

Figure S6. Related to Figure 6

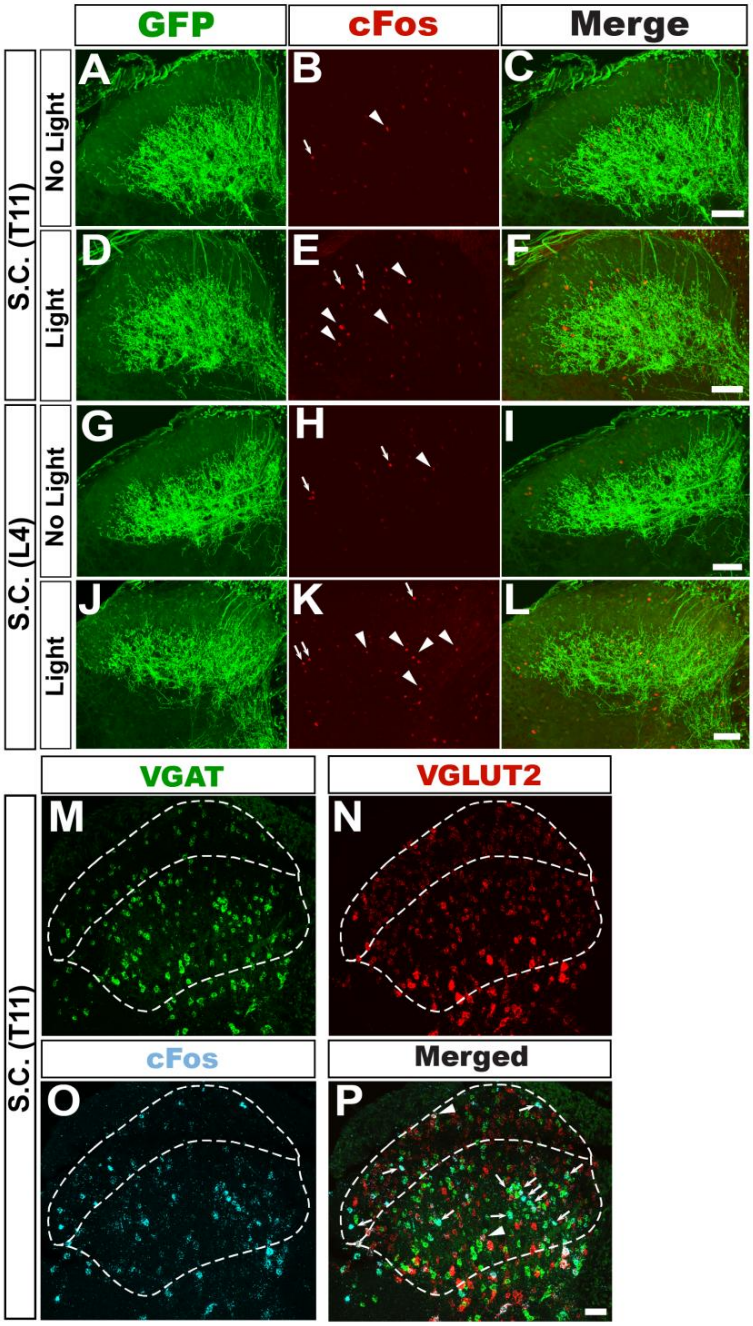

3. Supplementary Figure Legends

Supplementary Figure 1. Histological characterizations of *Split^{Cre}-Aβ ReaChR* mice, related to Figure 1.

(A) Schematic depicting the genetic configuration of the *Split^{Cre}* mouse line. (B) Schematic depicting the breeding strategy to generate *Split^{Cre};Advil^{FlpO};Rosa$^{ReaChRf/+}$* triple mice. (C-E) Images of dermal papilla sections of the plantar skin showing GFP^{+} nerves are NF200^{+} and innervate S100^{+} Meissner's corpuscles. GFP^{+} fibers rarely innervate the K8^{+} Merkel cell at the base of papilla. (F) Quantification of the percentage of GFP^{+} peripheral axons innervating Meissner's corpuscles. Data are presented as Mean ± SEM. 6-8 sections/mouse, n = 4-6 mice. (G) Whole-mount immunostaining of the hairy back skin showing that GFP^{+} peripheral axons are NF200^{+}. (H-J) Whole-mount immunostaining of the hairy back and tail skin showing that GFP^{+} peripheral axons are NF200^{+}. A few GFP^{+} fibers innervate Merkel cells in the hairy skin (an example indicated by a white arrowhead). n = 4-6 mice. (K-N) Whole-mount immunostaining of the hairy back, nape and posterior ear skin showing that GFP^{+} peripheral axons are NF200^{+} and form lanceolate ending structures around hair follicles.

Supplementary Figure 2. Histological characterization of *Split^{Cre}-Aβ TauDTR* mice, related to Figure 2.

(A) Immunostaining of a lumbar DRG section showed a little overlap between tdTomato$^+$ DRG neurons and nociceptor markers CGRP or IB4. (B) Immunostaining of DRG sections showing high overlaps between tdTomato$^+$ DRG neurons and a large-diameter neuron marker NF200. White arrows indicate some overlapped neurons. (C) Immunostaining of DRG sections showed some overlap between tdTomato$^+$ DRG neurons and a proprioceptive marker PV. (D) Quantification of the percentage of tdTomato$^+$ neurons expressing different markers. 6-8 sections/mouse, n = 4-6 mice. Error bars represent Mean ± S.E.M. (E) Immunostaining of a lumbar spinal cord section showing laminar segregation of tdTomato$^+$ central terminals and CGRP$^+$ or IB4$^+$ nociceptor terminals. (F) Immunostaining of a lumbar spinal cord section showing tdTomato$^+$ central terminals innervate deeper dorsal horn lamina (III-V), indicated by VGLUT1$^+$ staining. (G-I) Immunostaining of plantar skin sections showed that tdTomato$^+$ peripheral axons are NF200$^+$ and innervate Meissner's corpuscles (revealed by S100 staining) but rarely innervate K8$^+$ Merkel cells. White arrows indicate some Meissner's corpuscles, while white arrowheads indicate some Merkel cells. 6-8 sections/mouse, n = 4-6 mice. (J) Whole-mount immunostaining of the hairy back skin shows that tdTomato$^+$ peripheral axons are NF200$^+$. (K) Whole-mount immunostaining of the hairy back skin showed that most of tdTomato$^+$ peripheral axons are NF200$^+$, and a

few tdTomato$^+$ fibers also innervate Merkel cells (One example indicated by a white arrowhead). (L-N) Whole-mount immunostaining of the nape, posterior ear and back skin showing that tdTomato$^+$ peripheral axons form lanceolate endings around the hair follicles of different hairy skin regions. (O) Quantification of total tdTomato$^+$ fibers innervating dermal papilla per footpad section showed a significant decrease with DTA-treatment ($p = 0.0022$), 5-7 sections per mouse, n = 6 mice. Error bars represent Mean ± S.E.M. Unpaired, two-tailed Mann-Whitney test. $^{**}p < 0.01$

Supplementary Figure 3. Ablation of Split^{Cre}-Aβ-LTMRs did not alter general locomotion, and thermal sensation, related to Figure 3.

(A) Ablation of Split^{Cre}-Aβ-LTMRs did not alter the time spent in peripheral ($p = 0.38$) and central zones ($p = 0.328$) in vehicle vs DTA treated mice. There was also no difference in total distance travelled between the two groups ($p = 0.72$). (B) No difference in baseline heat nociception sensitivity, indicated by the latency of hind paw flick ($p = 0.64$), hind paw lick ($p = 0.904$), or jump ($p = 0.733$), in the DTA vs vehicle treated groups in static hotplate test. (C) No difference in baseline heat nociception sensitivity, indicated by the heat pain temperature threshold ($p = 0.702$) between the DTA vs vehicle treated using the dynamic hotplate test, n = 8 mice in each group in (A-C). (D) No difference in baseline cold nociception sensitivity, indicated by the paw-withdrawal

latency ($p = 0.395$) to dry ice, between the DTA vs vehicle treated groups, n = 9 mice in each group. (E) Representative images of hook (a) and loop (b) material of the Velcro surface. Scale bar = 0.5 mm. Error bars represent Mean ± S.E.M. Unpaired, two-tailed Mann-Whitney test. *$p < 0.05$, **$p < 0.01$; ***$p < 0.001$, ns = non significance, BL = baseline.

Supplementary Figure 4. Ablation of Split^{Cre}-Aβ-LTMRs altered the gentle touch and nociception in the hairy skin, related to Figure 3.

(A) Illustration showing cutaneous sensory afferents of the ablated hairy skin; green fibers represent nociceptive C/Aδ fibers; red fibers represent RA Aβ-LTMRs encircling the hair follicles; black fibers represent SA Aβ-LTMRs innervating Merkel cells (black bead-like structures); blue and brown colored fibers represent the C- and Aδ-LTMRs respectively; 'X' symbol represents the DTA-induced selective ablation of Split^{Cre}-Aβ-LTMRs. (B) The ablated mice showed significantly increased scratching behaviors in response to a tape attached to the back ($p = 0.0027$). (C) In response to a tape attached to the back, no difference in licking behaviors between the vehicle and DTA groups ($p = 0.743$) was observed. (D) The ablated mice displayed significantly increased number of licking episodes ($p = 0.0074$) in response to the application of an alligator clip at the nape of the neck. n = 11 and 10 mice in vehicle and DTA groups respectively in (B-D). Also see the supplementary

video 3. Error bars represent Mean ± S.E.M. Unpaired, two-tailed Mann-Whitney test. **p < 0.01.

Supplementary Figure 5. Local optogenetic activation of Split^{Cre}-Aβ-LTMRs at different skin areas, and CFA-induced inflammation alter the GFP^{+} fiber innervation in plantar skin, related to Figure 4.

(A) Schematic showing how blue laser was shined to stimulate different skin areas of the *Split^{Cre}-Aβ ReaChR* mouse. (B) *Split^{Cre}-Aβ ReaChR* mice showed high responsive rates to different intensities (5, 10 and 20 mW) of blue laser stimuli on different hairy skin (Nape of the neck, back and tail) regions. (C) The tail-flick latency decreased significantly in an intensity dependent manner (5 mW vs 10 mW, p = 0.005); (5 mW vs 20 mW, p = 0.0008); (10 mW vs 20 mW, p = 0.68). n = 8 mice in (B-C). Error bars represent Mean ± S.E.M. One way ANOVA followed by Tukey's multiple comparison. *p < 0.05, **p < 0.01, ***p < 0.001, ****p < 0.0001. (D-E) Triple staining of GFP, NF200 and K8 with plantar footpad sections of control and CFA-treated *Split^{Cre}*-Aβ *ReaChR* mice at post-CFA Day 7. (F-G) Double staining of GFP and S100 with footpad sections of control and CFA-treated *Split^{Cre}-Aβ ReaChR* mouse at post-CFA Day 7. (H) Quantification of Merkel cell numbers per foot pad skin section showed no significant difference between the control and CFA treated mice (p = 0.179) at post-CFA Day 7. (I) Quantification of the percentage of GFP^{+} fibers innervating

Merkel cells per foot pad section showed a non-significant increase trend in CFA treated mice, compared to the control ($p = 0.088$). (J) Quantification of the number of Meissner's corpuscles per foot pad section showed non-significant decrease trend in control and CFA-treated mice ($p = 0.0931$). (K) Quantification of the percentage of GFP^+ fibers innervating Meissner's corpuscles per foot pad section showed a significant decrease in CFA treated mice compared to the control ($p = 0.041$), n = 6 mice in each group (5-7 sections per mouse. (L) Results showing the effect and time course of the neuropathic medial plantar nerve ligation (MPNL) model. Control mice undergone MPNL showed a significant decrease in the 50% PWT ($p < 0.0001$), which didn't recover as the experiment lasted up to D28, n = 9 mice. Error bars represent Mean ± S.E.M. Mann-Whitney test in H-K & One way ANOVA followed by Bonferroni's test in L and M. *$p < 0.05$, **$p < 0.01$, ****$p < 0.0001$.

Supplementary Figure 6. Dorsal column activation of $Split^{Cre}$-$ReaChR^+$ Aβ-LTMRs evoked spontaneous behaviors and c-Fos expression in deep dorsal horn neurons, related to Figure 6.

(A-C) Double immunostaining of c-Fos and GFP with a T11 spinal cord section of an unstimulated *$Split^{Cre}$-Aβ ReaChR* mouse showing innervation of ReaChR-$EFYP^+$ central terminals in the layer III-V and baseline c-Fos expression. (D-F) Double immunostaining of c-Fos and GFP with a T11 spinal

cord section of a light-stimulated *Split^{Cre}-Aβ ReaChR* mouse showing innervation of ReaChR-EFYP^{+} central terminals in the layer III-V and increased c-Fos expression. (G-I) Double immunostaining of c-Fos and GFP with a L4 spinal cord section of an unstimulated *Split^{Cre}-Aβ ReaChR* mouse showing innervation of ReaChR-EFYP^{+} central terminals in the layer III-V and baseline c-Fos expression. (J-L) Double immunostaining of c-Fos and GFP with a L4 spinal cord section of a light-stimulated *Split^{Cre}-Aβ ReaChR* mouse showing innervation of ReaChR-EFYP^{+} central terminals in the layer III-V and increased c-Fos expression. White arrowheads indicate some examples of c-Fos immunoreactivity in deeper laminae. White arrows point to some c-Fos^{+} cells in superficial laminae of the dorsal horn. n = 3 mice in each group (5-7 sections per mouse for statistical comparison). (M-P) Representative images of RNAScope *in situ* hybridization for *Vgat*, *Vglut2* and *c-Fos* with a T11 spinal cord section of a spinal light-stimulated *Split^{Cre}-Aβ ReaChR* mouse. White arrowheads indicate some examples of co-localized VGLUT2^{+} and c-Fos^{+} neurons. White arrows indicate some co-localized VGAT^{+} with c-Fos^{+} neurons. n = 3 mice (3-4 sections per mouse). Error bars represent Mean ± S.E.M. Mann-Whitney test. *$p < 0.05$, **$p < 0.01$, ***$p < 0.001$.